Development of a catalyst dip-coating process for a catalytic plate reactor

Pakpong Roongruangsree

Supervised by: Prof. Jan Kopyscinski

A thesis submitted to McGill University in partial fulfillment of the requirements for the degree of

Master of Engineering

Department of Chemical Engineering

McGill University, Montreal

Acknowledgement

I would like to thank my supervisor Professor Jan Kopyscinski for accepting me into his research group and guiding me with my research. I must also extend my gratitude to my Catalytic process Engineering research group members who helped me with sample processing and provided me with excellent advice: Kanchan Dutta, Jennifer Martin del Campo, Lizbeth Moreno Bravo, Alexandra Jacobson, and especially Jose Augusto Hernandez Lalinde who taught me how to operate the CPR and everything I needed to know about catalysis. This research would not have been possible without your help. Moreover, I appreciate the work of the technicians, namely Ranjan Roy, Andrew Golsztajn, David Liu, and Aleksandra Djuric, who characterized the samples for this research. Finally, I am grateful to Xebec Adsorption Inc. who provided funding and catalyst samples for the project.

I owe my Master's degree academic life at McGill University to the funding from the Royal Thai government scholarship. Not only did the Thai government scholarship pay for my tuition fees and spending, it is also one of the reasons I was accepted to McGill University in the first place. Lastly, my gratitude goes out to my parents who always supported and inspired me to continue my academic journey abroad. I am thankful to all the people involved in my research thesis and I hope I can use the knowledge I gained in this work to improve myself as a researcher and as a person. I hope I am making you all proud.

Graphical Abstract

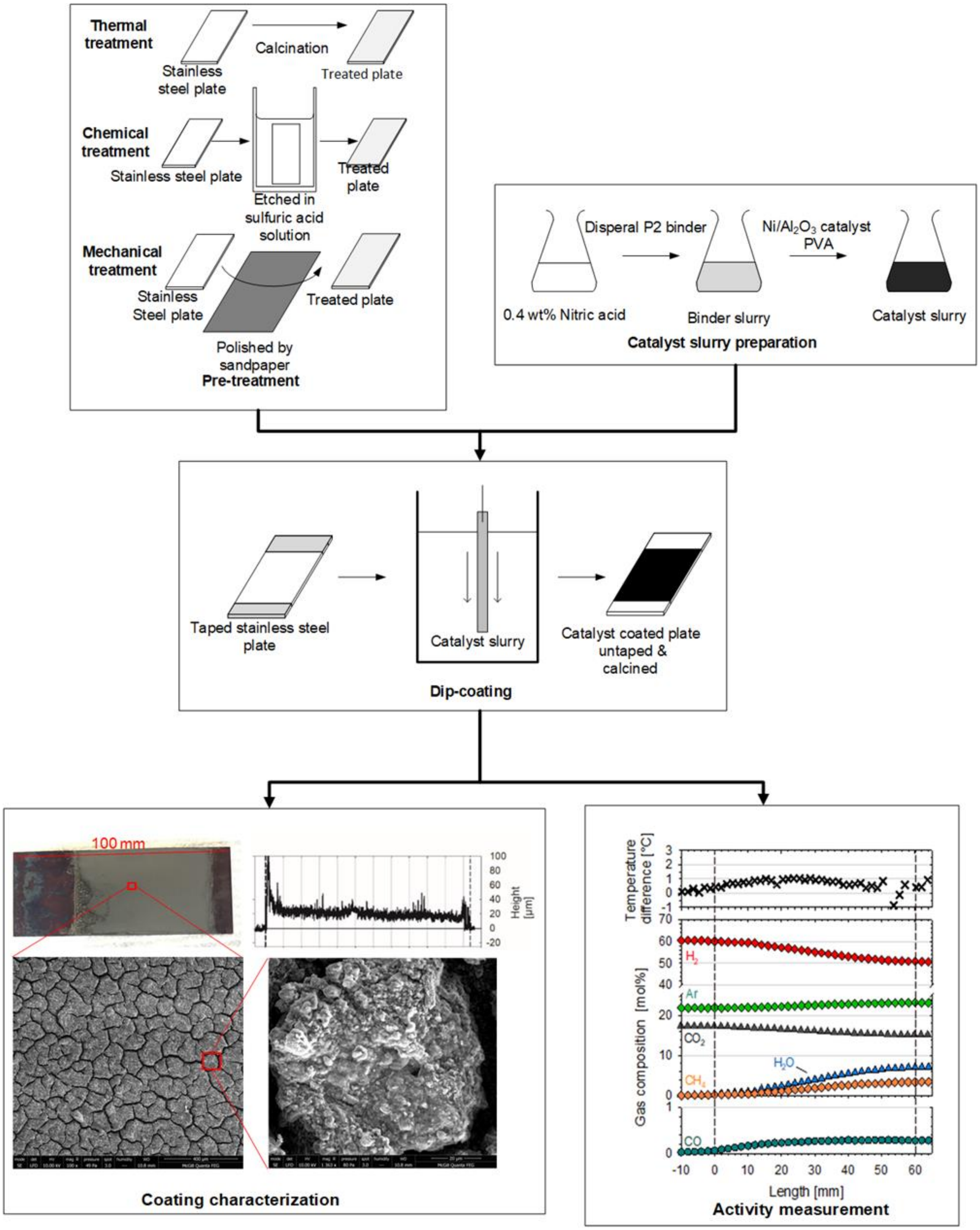

Abstract

The Catalytic Process Engineering research group developed a catalytic channel reactor with spatially-resolved measurement capabilities to study the CO_2 methanation reaction. The bottom plate of the reactor is coated with a catalyst of interest, while the top is closed with a quartz glass plate to enable temperature measurements of the catalyst surface via infrared thermography. In addition, the reactor is equipped with a small movable sampling capillary to determine the gas composition along the reactor axis.

The goal of this thesis research was to develop and optimize a dip-coating procedure that yields a homogenous coating with a known catalyst mass distribution using a commercial Ni-based catalyst. Stainless steel was chosen for the substrate plate that will be used in the channel reactor. Stainless steel is more economical than other substrates such as ceramics and Fe-Cr alloys. Moreover, stainless steel is chemically inert towards the methanation reaction and has a high heat conductivity.

This study focused on the optimization of a dip-coating method, which encompasses pretreatment of the plate, catalyst slurry preparation and subsequent coating. For that purpose, three pre-treatment methods as well as different catalyst particle sizes and slurry recipes (i.e., ratio of catalyst, binder and solvent) were investigated. The best coatings in terms of loading and homogeneity were achieved by using the chemically treated plates, which produced the highest surface roughness in combination with slurries containing catalyst particles of less than 20 μm and polyvinyl alcohol. Dip-coating experiments showed that multiple dip-coating steps with intermediate calcination at 100°C yielded the most homogenous coating. The catalyst coating was mechanically stable for more than 500 h under thermal conditions up to 400°C. The best coating was tested in a catalytic plate reactor under CO_2 methanation conditions. The coating activity along the reactor axis over a wide range of reaction temperatures was nicely illustrated by the results.

Résumé

Des réacteurs à plaques ou à canaux sont utilisés pour étudier la méthanisation du CO_2. Le réacteur est constitué d'un catalyseur placé sur une plaque servant de support. L'objectif de cette recherche est de produire une plaque enrobée de catalyseur de manière homogène. Il a été prouvé que des catalyseurs commerciaux à base de Ni catalysent la réaction de méthanisation. Dans cette étude, de l'acier inoxydable est choisi comme plaque de support pour le catalyseur. En effet, l'acier inoxydable est connu pour être économiquement viable quant au transfert de procédé à grande échelle et chimiquement inerte. Différentes méthodes de revêtement catalytique existent telles que le revêtement par immersion ou par brossage. Cette étude se concentre sur l'investigation et l'optimisation du revêtement par immersion. Trois méthodes de prétraitement de l'acier inoxydable ont été étudiées : thermale, mécanique et chimique. La surface la plus rugueuse (±2.5 um) a été obtenue par traitement chimique. Différentes méthodes de préparation de la suspension de catalyseur ont également été étudiées. Une charge de catalyseur de 3.37 mg cm-1 a été obtenue en utilisant une suspension constitué d'un mélange de catalyseur Ni sur de l'alumine, un liant à base d'alumine et du polyvinyle d'alcool. Les expériences ont montré que le revêtement catalytique le plus régulier et homogène a été obtenu par une succession d'immersions en effectuant une calcination modérée à 100°C entre chaque immersion. Ce revêtement catalytique a ensuite été testé dans un réacteur à plaques : le dioxyde de carbone et l'hydrogène sont convertis en méthane par la réaction de méthanisation comme attendu.

Content

Chapter 1

1 Introduction

1.1 Motivation

The primary source of power worldwide is currently fossil fuels. This heavy usage of fossil fuels has led to an increase in carbon dioxide (CO_2) emissions into the atmosphere, contributing to the global warming effect. Alternatively, various renewable energy technologies such as solar, wind, biomass, and hydro have been developed to counter the problem. These technologies were created as more environmentally friendly and more sustainable alternatives to fossil fuels. However, these renewable energy technologies such as wind and solar power are unable to produce energy on demand as they are limited by environmental factors. For example, solar panels can only produce energy on sunny days and wind turbines function only when a significant air flow is available. This creates variations on the produced electrical grids and subsequently creates a gap between energy supply and demand.

With these fluctuations in power produced, energy storage has become very crucial to answer the constant demand of power [1].

Power-to-gas (P2G) is one of the most promising energy storage technologies as it allows for the storage of large capacities of energy in the form of gas. Furthermore, P2G also has a larger discharge time when compared to other currently used energy storage technologies such as batteries and hydro storage as shown in Figure 1-1 [2].

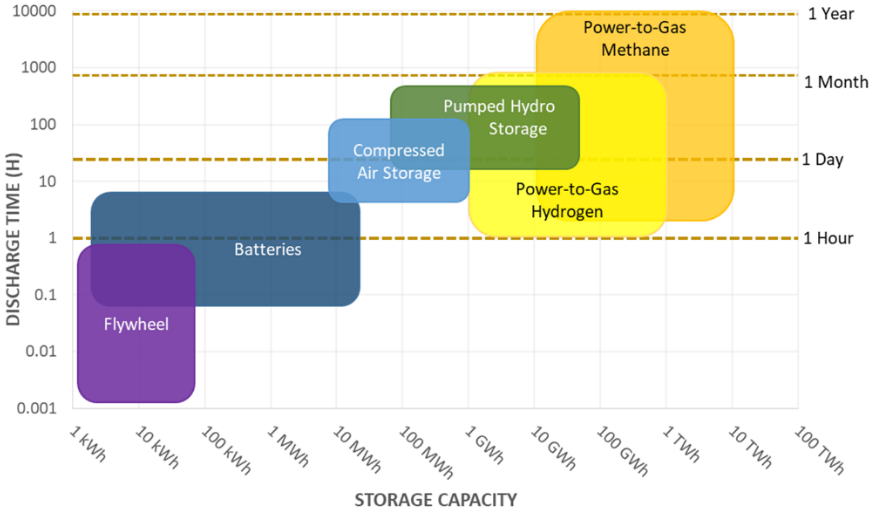

Figure 1-1 Comparison of discharge time and storage capacity of various storage technologies modified from [3].

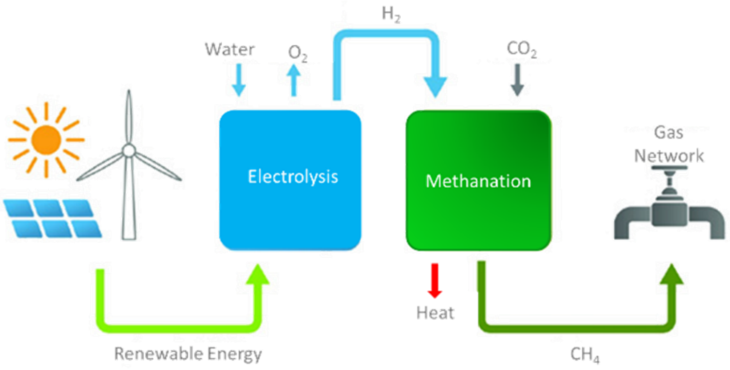

Figure 1-2 Methane power-to-gas process flow chart.

As shown in Figure 1-2, the P2G process converts electrical energy from renewable energy sources to hydrogen (H_2) via water electrolysis producing an oxygen (O_2) byproduct. Hydrogen can already be used to provide energy for fuel cells or internal combustion engines. However, current energy infrastructure is still unable to fully adopt the use of hydrogen as an energy storage gas due to storing difficulties. Hydrogen can be further converted to methane (CH_4) via the methanation of carbon dioxide [4], [5]. Unlike hydrogen, methane already has supported natural gas infrastructure in place. Natural gas distribution network also has a higher energy discharge time and storage capacity when compared to other technologies (Figure 1-1). Captured CO_2 can come from various sources such as biogas, industrial processes or even from the atmosphere [6]. The combination of P2G and carbon capture technologies would answer the problems of CO_2 emission and energy storage simultaneously.

Methanation is usually carried out in catalytic adiabatic fixed bed reactors. However, they have inherently some disadvantages such as non-isothermal behavior and little flexibility in terms of turndown ratio and startup time. Fixed bed reactors might be feasible for large and continuous operation, however, the P2G process requires a reactor and process concept optimized for small scale (e.g., biogas plant) and dynamic operations (rapid shut-down and start-up). The latter is important when the electrolyser does not generate sufficient H_2 due to intermittent production of renewable electricity. Until now, no small scale and flexible (20-1000 $m^3 h^{-1}$) reactor concepts were commercially available.

The catalytic process engineering (CPE) group led by Prof Kopyscinski proposes a catalytic heat exchange / channel reactor type of configuration (Figure 1-3). The channel reactor is made of multiple layers of catalyst coated metal substrate plates stacked together with small channels between them for the reactant gases to flow through. This design can easily be scaled up by adding more coated plates to the reactor or scaled down by removing plates. It also possesses great heat and mass transport properties and is very compact [7], [8]. The versatility of the prototype channel reactor would be beneficial when the methanation reaction is scaled up to an industrial level as the volume size of the reactor can be tailored to match the amounts of reactant gases and desired products.

There are already reported uses of Fe-Cr alloys and ceramics as the substrate for catalyst coated reactors. However, stainless steel was selected for the purpose of this research. In comparison to Fe-CrAl-loys and ceramics, stainless steel is cheaper while still possessing a suitable thermal conductivity and chemical stability for a substrate plate. This makes stainless steel the more economically favorable alternative in large scale methanation processes. For the catalyst, nickel is cheaper than other suitable metals used for the methanation reaction such as Ru and Fe [9]. Nickel catalysts are also commercially available, usually in the form of Ni on an alumina support (Ni/Al_2O_3).

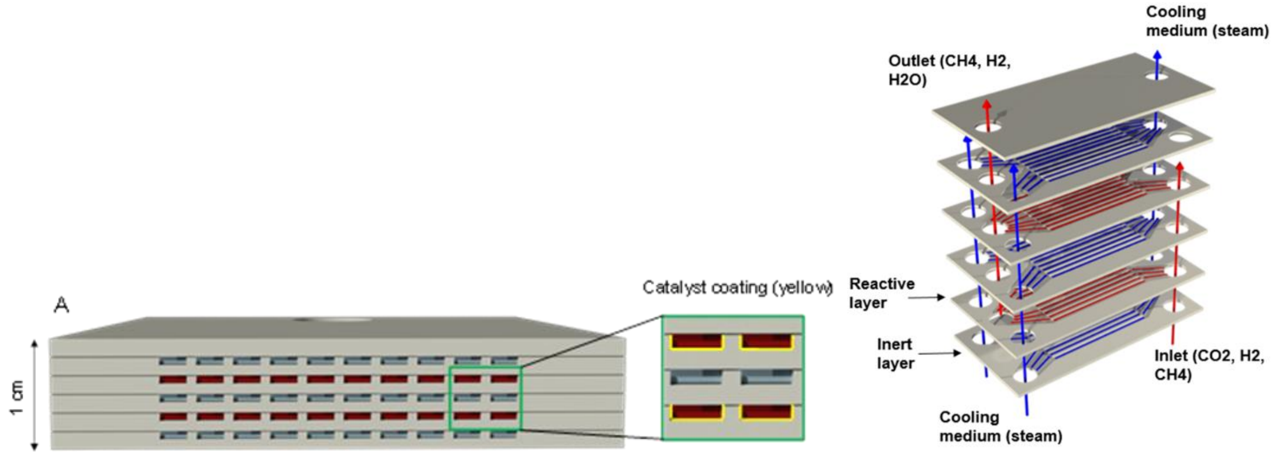

Figure 1-3 (Left) Cross-section view of possible prototypical micro-channel reactor models, (Right) Flow of reactant gases [10].

The purpose of this research was to develop a coating method to deposit a commercial nickel catalyst onto a stainless steel substrate plate. There are already several existing coating methods such as frame coating and spin coating. However, this thesis focuses on the dip-coating, which requires the substrate plate to be submerged in a catalyst slurry and pulled out at a certain speed. The advantage of this dip-coating method is that it coats both sides of the substrate plate simultaneously and only requires one large batch of prepared catalyst slurry to coat multiple substrate plates. Subsequently, methods that involved the coating of the Ni catalyst onto the stainless steel plate were studied. These studies included pre-treatment of the stainless steel plates, Ni catalyst slurry preparation, and dip-coating of stainless steel plates into the catalyst slurry.

1.2 Objectives

The objective of this study was to develop a dip-coating procedure for ready-made (commercially available) Ni-alumina catalysts. This included the pre-treatment for AISI 420 stainless steel substrate plates, the preparation of a catalyst slurry, and dip-coating itself.

The following questions were investigated in this report:

1. What pre-treatment methods achieve highest catalyst loading after the dip-coating process?
2. How does catalyst particle size effect the catalyst loading of the substrate plate?
3. What are the effects of multiple dip-coating methods on a single stainless steel plate?
4. Are the coated plates suitable for use in catalytic plate reactors to study CO_2 methanation?

1.3 Organization of the thesis

This thesis can be divided into three main sections: theoretical background, explanation of the experimental procedure, and the report and discussion of the results.

Chapter 2 provides background on the development of coated channel reactors, their substrates and catalyst slurry preparations.

Chapter 3 lists the experiments done in the investigation of stainless steel pre-treatment, catalyst slurry preparation, dip-coating, and characterization of the catalyst slurry.

Chapter 4 presents the results and discussion of the experiments as listed in chapter 3

Chapter 5 concludes the investigation and provides direction on further experiments for future research.

1.4 Contributions

It was the thesis author's responsibility to research and review literature for the experimental designs. The author was also responsible for conducting the experiments, analyzing the data and discussing the results under the supervision of Professor Jan Kopyscinski.

Chapter 2

2 Theoretical background

Ever since the carbon oxide (CO, CO_2) methanation reaction was first discovered by Sabatier and Senders in 1902, it has been continuously investigated by numerous researchers [11]. This reaction's thermodynamic properties, reaction mechanism, possible catalysts and kinetics have been summarized in various reviews and articles. This chapter provides a background from literature on the methanation reaction, reactor materials, catalysts, and coating methods.

2.1 CO_2 methanation

During CO_2 methanation, three main reactions take place which are listed as Rx 1 to 3. The first reaction occurs when CO_2 reacts with H_2 to form CH_4 and H_2O. However, CO_2 can also be converted to CO and H_2O via a competing reverse water gas shift reaction (Rx 2). This undesired CO can be further converted to CH_4 via Rx 3. Reactions Rx 1 and Rx 3 are highly exothermic and thermodynamically favored at low temperatures and high pressures. The reverse water gas shift reaction (Rx 2) is endothermic. Rx 1 is the main reaction, while Rx 2 acts as a competing reaction.

$$CO_2 + 4H_2 \rightarrow CH_4 + 2H_2O \qquad \Delta H_R^o = -165\ kJ\ mol^{-1} \tag{Rx 1}$$

$$CO_2 + H_2 \leftrightarrow CO + H_2O \qquad \Delta H_R^o = 41\ kJ\ mol^{-1} \tag{Rx 2}$$

$$CO + 3H_2 \leftrightarrow CH_4 + H_2O \qquad \Delta H_R^o = -206\ kJ\ mol^{-1} \tag{Rx 3}$$

2.2 Catalyst and substrates

There are three main variables that must be taken into account when creating a functional catalytic plate. These include (1) the catalyst material, (2) the substrate plate material, and (3) the catalyst deposition method. A catalyst is typically needed for the methanation reaction to decrease the reaction's large energy barrier. In this thesis, the term "substrate" was chosen to denote the stainless steel reactor plate. Additionally, for the sake of clarification, the term "support" refers only to the catalyst support material (i.e., Al_2O_3) that provides surface area and mechanical strength. The support interacts with the substrate to create a strong and homogenous catalyst coating as depicted in Figure 2-1 [12], [13]. In addition to the catalyst and the substrate, binders and supporting materials are often used to promote homogeneity and adhesion between the catalyst and the substrate plate [14].

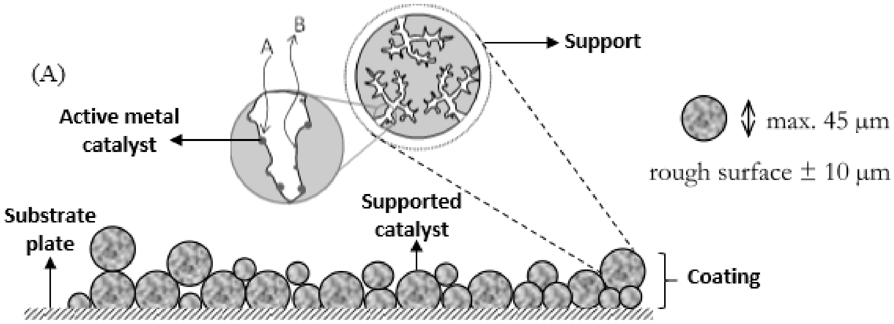

Figure 2-1 Schematic of substrate plate coated with catalyst. Adapted from [13].

The following sections provide a brief background on different methanation catalysts and substrate plates. A small review about the coating procedure including plate pre-treatment and coating is also included.

2.2.1 Catalyst

There exist many commercially available metal catalysts capable of catalyzing the CO and CO_2 methanation reactions. The most commonly used metals are Ru, Ni, Co, Fe, and Mo [9]. These metals are usually dispersed into a supporting material such as Al_2O_3, SiO_2, TiO_2, ZrO_2, or CeO_2 to increase the surface area of the catalyst [15]. In 1975, Vannice reported a list of pure metal catalysts dispersed on Al_2O_3 that could be used for catalyzing the CO methanation reaction with the following activities trend: $Ru \gg Fe > Ni > Co > Rh > Pd > Pt > Ir$ [16]. Among the listed metal catalysts, Ruthenium (Ru) catalysts provide the highest activity but are unsuited for large scale methanation due their elevated cost [9]. Molybdenum (Mo) catalysts are known for their resistance to sulfur with moderate activity. However, they require high reaction temperatures, which a catalytic plate reactor may not be able to provide. Cobalt (Co) and iron (Fe) catalysts have acceptable activities but risk plugging and bridging of the reactor due to an increased carbon deposition [9].

For this thesis, it was concluded that Nickel (Ni) was the optimal choice of metal catalyst for CO_2 methanation. It is cheaper than Ru and Mo, yet still provides sufficient catalytic activity for the reaction to progress. However, unlike Mo based catalysts, Ni catalysts can experience catalyst deactivation due to sulfur poisoning. Furthermore, like with Co and Fe catalysts, carbon deposition can occur if proper reaction temperatures are not used, if excess H_2 is present in the feed, or if the Ni is not adequately supported using metals oxides [17], [18]. Subsequently, Ni supported on Al_2O_3 (Ni/Al_2O_3) is amongst the most studied catalysts for the methanation reaction due to its high performance per cost ratio [15], [18]–[20]. Therefore, Ni/Al_2O_3 was chosen as the catalyst for the entirety of this research thesis.

2.2.2 Substrate plate

The parameters and conditions needed for the CO_2 methanation reaction would determine the substrate material for the catalytic plate. The ideal substrate plate material should fulfill the following requirements:

1. Chemically inert toward methanation
2. Can be easily coated with the catalyst
3. High heat conductivity
4. Able to withstand thermal shock
5. Economical

The first possibility is to use a FeCrAl alloy (Fecralloy^{TM}) for the substrate plate. This metal alloy contains 72.8% Fe, 22% Cr, 5% Al, 0.1% Y, and 0.1% Zr [21]. Fecralloy possess excellent oxidation resistance at high temperatures up to 1300-1400°C [22]. They also possess a high thermal conductivity. There are many reported uses of Fecralloy as a substrate due to its good heat transfer and resistance. However, catalyst coatings often experience difficulties adhering to Fecralloy plates. To counter this problem, additional treatments of the catalyst in the form of crushing, sieving, and the addition of binder are required [23], [24].

A second choice for the substrate plate is the use of ceramics such as metal oxides (Al_2O_3, Ce_eO_3), metal nitrides (Si_3N_4) and carbides (SiC) [25]. Ceramics have excellent stability under high temperatures and a good resistance to thermal shock. However, it is difficult to disperse catalysts over ceramic surfaces due to their low porosity and surface area [26]. Thus, an inorganic oxide washcoat layer must often be deposited onto the ceramic surface prior to coating the catalyst.

While both Fecralloys and ceramics have been reported as functional substrate materials for small scale laboratory reactors, they are quite expensive and economically unsuitable for large scale systems. Stainless steel is a suitable and cheap alternative. This steel alloy contains at least 10.5% chromium mixed with other metals such as Ni and Mo to enhance its mechanical properties, making it resistant to oxidation and corrosion [27]. Normally, stainless steel has a thin layer of chromium oxide protecting it from corrosion. It also has very good heat transfer properties. Due to its lower price and comparable properties to the aforementioned materials, stainless steel is a desirable substrate material. One of the objectives of this thesis was to test stainless steel as a substrate plate for methanation in order to determine its viability towards the construction of a prototype channel reactor [10].

2.3 Pre-treatment methods

In order to deposit catalyst particles onto the surface of a substrate plate and create a homogenous coating, the substrate plate must first be pre-treated. The purpose of this process is to increase the surface roughness thereby promoting the adhesion of the catalyst particles. In this thesis, three methods of pre-treating stainless steel substrate plates were tested: thermal treatment, chemical treatment, and mechanical treatment.

2.3.1 Thermal-treatment

Thermal pre-treatment is a thermal oxidation process occurring at elevated temperatures used to form thin films of metal oxide. While stainless steel can withstand oxidation over a temperature range of 100-500°C, it can still be oxidized when subjected to higher temperatures for a prolonged period of time. Oxidation is commonly performed using air [17] or oxidizing gases. Fecralloy substrates usually undergo thermal treatment unlike ceramics which display a lower affinity for thermal oxidation [28]. With regards to stainless steel, γ-Fe_2O_3 (Austenite) and Fe_3O_4 (Ferrite) can be formed during the oxidation process in the temperature range of 600-900°C [29]. The amount of chromium in stainless steel influences the properties of the material during oxidation and phase changes. For example, austenite can swell at 900°C leading to nodule formation. The formation of these nodules and swellings is caused by the breakaway oxidation of a chromium depleted layer and limits the lifetime of the reactor [30]. Therefore, stainless steel should not be thermo-treated at high temperatures for prolonged duration of time. Thermal treatment was aimed towards increasing the surface roughness of the substrate plate for the catalyst particles to be deposited on. This in turn promotes the durability of the catalyst coating.

2.3.2 Chemical treatment

Rather than heating the substrate plates as per thermal-treatment, chemical treatment utilizes the chemical reactions that occur when a substrate plate is submerged in acid to start the oxidation reaction. The acid not only increases the substrate’s surface roughness allowing the catalyst to be deposited onto the substrate, but it also rids the substrate plate of impurities improving the quality of the catalyst coating [31]. Another advantage of chemical treatment is that the substrate plates do not bend like they do in thermal-treatment. However, chemical treatment requires the use of strong acids that must be disposed of properly.

In 2006, Giornelli et al. experimented on the pre-treatment of stainless steel plates using a sulfuric acid solution [32]. The plates were etched in a 30 wt% sulfuric acid solution for 2 hours to increase the roughness of the substrate surface. To clean the plates, they were then sonicated twice in water for 30 min and left to dry at room temperature. The composition of the stainless steel plates remained unchanged after acid treatment, but the surface roughness increased after acid treatment (Figure 2-3).

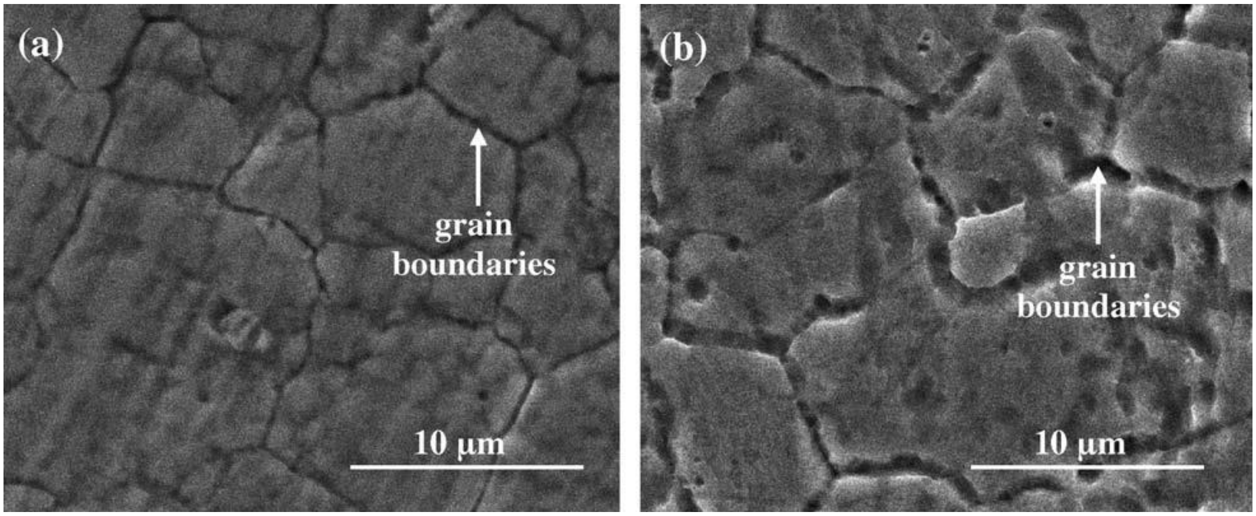

Figure 2-1 SEM micrographs (x5000) of Giornelli et al. stainless steel surfaces before (A) and after (B) acidic treatment [29].

2.3.3 Mechanical treatment

Unlike the previous pre-treatment methods, mechanical treatment does not involve oxidation. There are reports of using mechanical methods to increase the substrate surface roughness without requiring the oxidation reaction. In this case, the surface of the substrate is scratched by an abrasive material such as sandpaper or other fine particles. The advantage of this method is that it does not require any acid etching or calcination at high temperatures, saving both resources and time. The surface roughness for catalyst deposition would be increased solely due to mechanical means.

Sarwani et al. outlined a method for pre-treating grade 304 stainless steel plates by polishing them with sand paper [33]. The dimensions of the stainless steel plates were 15 x 60 x 0.5 mm. They were sanded using an abrasive paper (grit 400). In their work, the stainless steel plates were polished for 30 cycles in one direction before being coated with Ni-Alumina catalyst. The coated plates were later calcination at 300-600°C. The study showed trends of increasing surface roughness (56-275 nm) and thickness (581-1898 nm) of the coating with increasing calcination temperature (300-600°C). A similar method was described by Barati et al. Stainless steel plates with dimensions of 20 mm width x 15 mm length x 5 mm 316L were polished using No. 80–1500 emery papers followed by 0.3 and 0.05 mm alumina powders [34]. The plates were later dip-coated in TiO_2 sol-gel solution. Their study achieved maximum coating thickness of ~3,000 nm with 400°C post-calcination temperature and 30 cm min^{-1} pull speed. For this thesis, the method of Sarwani et al. was adopted by using 400 grit sandpaper as the means of mechanically treating the substrate plates [33].

2.4 Coating procedure

Catalyst deposition onto the substrate surface can be very complex due to variations between each specific catalyst and substrate pair [35]. The procedure primarily involves the deposition of the supported catalyst. Only in some specific cases is the direct deposition of the active metal catalyst part of the process. In this research, commercially available and ready-made nickel catalysts that had been supplied by an industrial partner were used.

2.4.1 Deposition of supported catalyst

Catalyst suspension consists of preparing the supported catalysts in a liquid phase before coating them onto a substrate plate. The terms “suspension” and “slurry” are used to describe the solid catalyst suspended in a liquid phase which includes water, a binder and/or a solvent [14]. The binder plays a crucial role in improving the catalyst’s adhesion to the substrate by binding to both the catalyst particles and the substrate surface. There are many variables responsible for the quality of a catalyst coating such as particle size, pH, viscosity, and its electrochemical properties [17], [31].

The effect of catalyst particle size on catalyst coating quality was reported in the works of Agrafiotis et al. and González-Velasco et al. [36], [37]. Their works both concluded that adhesive coatings could be achieved by using small particles in the range of 2-10 μm. However, the achieved coatings became too dense and less active if the catalyst particles were too small [24]. On the other hand, if the particles were too large, the coatings became uneven. The shape of the particle surface area may also affect catalyst adhesion, though this effect may not be as pronounced as the influence of the particle size. This is because the substrate surface roughness (μm) is much larger than that of the catalyst particles (nm). Furthermore, catalyst slurries with higher viscosities would yield higher catalyst loadings but suffer from cracking during post-treatment calcination. This cracked and uneven catalyst layer can be prevented by using a more diluted and less viscous slurry, but this results in a lower catalyst loading. However, coating processes can be repeated to increase catalyst loading.

In 2009, Peela et al. proposed the use of poly vinyl alcohol (PVA) to control the viscosity of slurries [38]. Their work involved preparing a washcoat slurry to coat a channel reactor with γ-alumina by first creating a primer slurry using a 2% Disperal P2 alumina binder mixed with a 0.4 wt% nitric (HNO_3) acid solution. In 2015, Zhang et al. adopted Peela's method of preparing slurries and proposed a combination of primer and washcoat slurries [39]. γ-alumina (3 μm) and a catalyst would be directly added to the primer slurry. This method saved time and avoided the need to prepare two slurries simultaneously.

2.4.2 Dip-coating

There are many ways to quickly deposit a prepared catalyst slurry onto a substrate plate such as frame coating, spin coating, or spray coating [40]. However, these methods only allow the plate to be coated on one side at a time. Our research group's prototype channel reactor model requires each substrate plate to be coated on both sides. The dip-coating method allows for the plate to be coated on both sides simultaneously.

As its name suggests, dip-coating involves dipping a substrate plate into a catalyst slurry and leaving it submerged for a certain amount of time. Figure 2-4 shows a substrate plate being pulled out from the slurry with a certain speed, affecting the quality of the catalyst coating [17], [41], [42].

In 2016, Sarwani et al. experimented on the dip-coating method of a Ni-Alumina catalyst slurry on a grade 304 stainless steel plate [33]. The plate had the dimensions: 15 mm width, 60 mm length, and 0.5 mm thickness. The plate was dipped in and out of a catalyst slurry with a speed of 160 mm/min. Prior to the experiment, the stainless steel plate was cleaned using an ultrasonic cleaner and polished and sanded using abrasive paper with a grit of 400. To pre-treat the plate, it was polished in one direction 30 times to increase its surface roughness. Sarwarni provided an example of a mechanical treatment that was later adapted for this research thesis. His research also proved that dip-coating is a practical method for catalyst deposition achieving maximum Ni-alumina coating thickness of 1898 nm.

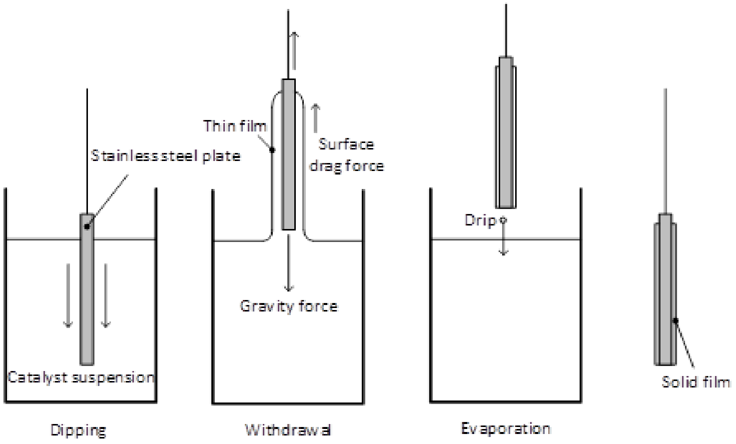

Figure 2-2 Steps of dip-coating process, modified from [34].

Barati et al. also studied the effect of a substrate's withdrawal speed on TiO_2 catalyst coating thickness [34]. For pre-treatment, 316 stainless steel plates with the dimensions of 20 x 15 x 5 mm were grounded and polished. The surface of the plates was cleaned using ethanol and acetone. The plates were then submerged into a TiO_2 catalyst slurry with varied withdrawal speeds of 3, 10, 15, 25 and 30 cm min^{-1}. The results showed that greater withdrawal speeds led to faster evaporation rates of the coating and accelerated gelation. It is also noted that coating drippings are less frequent at higher withdrawal speeds. This research showed the effects of varying the dip/pull speed of plates on the quality of the coating which will be further investigated in this research thesis. Higher pull-speed provided higher coating thickness as shown by maximum thickness of ~3000 nm was achieved by 30 cm min^{-1} while pull-speed of 3 cm min^{-1} achieved only ~30 nm coating thickness. However, it is noted that Barati's catalyst TiO_2 sol-gel solution had different catalyst and solvent components from this thesis research. Barati et al. used ethanol as part of solvent which was readily evaporated.

Kishida et al. prepared an $AgCl/Al_2O_3$ catalyst slurry with ultrasonic dispersion for 10 min to avoid any sedimentation before dip-coating [43]. If the coating powder was still sedimented on the bottom afterwards, the suspension was ultrasonically dispersed for another 10 min. A 10 x 10 mm substrate plate was dip-coated and later pulled up at a speed of 3 mm s^{-1}. The sedimentation of the catalyst particles indicated that the pulling speed must also be associated with the sediment speed of the particles. If the plate was pulled too quickly, catalyst loading would decrease. The dip-coating resulted in 4 µm catalyst coating thickness. Kishida's work reinforced the need to study the effect of the pull/dip speed of substrate plates while introducing an additional variable, the sedimentation speed of catalyst particles in the slurry.

2.4.3 Post-treatment

Finally, the catalyst coated substrate plates must be calcined as part of the post-treatment procedure. Parameters, such as temperature, duration of calcination, and heating rate influenced the quality of the final coating. Irregularities and cracking occur if inappropriate calcination parameters are used. Therefore, temperature profiles must be chosen in accordance to each catalyst and substrate.

Sarwani et al. studied the effect of calcination temperatures on the surface roughness of Ni-Alumina catalyst coatings on stainless steel substrate plates [33]. After each stainless steel plate was dip-coated, the plates were calcined for 90 min at temperatures ranging from 600-900°C. Sarwani reported that the surface roughness of catalyst coatings increased with calcination temperature. The catalyst film became increasingly rough and uneven at greater calcination temperatures.

Chapter 3

3 Experimental procedures

3.1 Materials

A commercial nickel catalyst supported on alumina (Ni/Al_2O_3, confidential catalyst manufacture) was used in this work. The catalyst, supplied by our industrial partner (Xebec Adsorption Inc.), was in the form of black pellets (~ 2 cm long, Figure A-1 in Appendices) with a >18 wt% Ni content. Disperal P2 (Sasol), an aluminum based-binder, was chosen to increase the adhesion of the catalysts onto the stainless steel plates. Disperal P2 binder is mainly comprised of boehmite (Al(OH)O). Polyvinyl alcohol (PVA) was purchased from Sigma Aldrich and was used in the development of the catalyst slurries. Stainless steel AISI 420 (Goodfellow) with dimensions of 20 x 20 cm and with a thickness of 0.5 mm was used for the substrate plates. The stainless steel plates were cut into 2 x 4 cm plates for small samples and 4 x 10 cm plates for larger samples.

3.2 Coating development

3.2.1 Pre-treatment of substrate plates

The effect of each pre-treatment method (thermal, chemical, and mechanical) was studied. Each method reshapes the surface in a different manner. Thermal and chemical treatments both cause surface oxidation. The former is achieved by heating the plate in the presence of oxygen while the latter results from a chemical reaction in acid. Mechanical treatment is performed to create physical alterations of the surface. The purpose of this section was to determine which of the aforementioned methods provided the greatest surface roughness on stainless steel plates.

3.2.1.1 Thermal treatment

Stainless steel plates were calcined in a muffle Furnace (MTI, KSL-1500X) at temperatures of 600, 700, 800 or 900°C. The plates were placed in the furnace, then heated at a rate of 5°C min^{-1} to the target temperature and calcined for 30 min at this temperature. After the furnace was cooled, the plates were then cleaned with DI water and isopropanol.

3.2.1.2 Chemical treatment

Stainless steel plates were etched in a 10, 20 or 30 wt% sulfuric acid (H_2SO_4) solution for 2 h. Parafilm was used to cover the beakers during the etching process with a small hole for ventilation present in the parafilm. Once complete, the plates were sonicated with DI water for 1 h and cleaned with isopropanol.

3.2.1.3 Mechanical treatment

Stainless steel plates were sanded using 400 grit sandpaper for 30 cycles in one direction. The samples were divided into two groups: plates polished in the axial direction and plates polished in the perpendicular direction. The plates were then cleaned with DI water and isopropanol.

3.2.2 Catalyst slurry preparation

Experiments were performed to optimize the catalyst slurry preparation process. Different slurries were prepared in order to study the effect of multiple variables such as solvent, slurry viscosity, catalyst particle size, solid to liquid ratio, and one-step versus two-step coating methods. Catalyst slurries were prepared by varying these parameters and then used in the dip-coating of stainless steel plates.

3.2.2.1 Sieving

Ni/Al_2O_3 catalyst pellets were crushed and sieved using a DUAL D-4326 motorized shaker and sieves. For this work, catalyst particles with < 20, 20-45 and 45-90 μm diameters were used for the coating process. Larger particles were not used, as pore diffusion may occur on their surface during chemical reactions. The Disperal P2 binder was also crushed and sieved.

3.2.2.2 Preparation of slurry for one step coating

Isopropanol based catalyst slurry

The first catalyst slurry was composed of a mixture of catalyst and Disperal P2 binder with a mass ratio of 9:1, as well as DI water and isopropanol with a volume ratio of 4:1 and a solid (g) to liquid (ml) ratio of 1 to 5.

Initially, Disperal P2 (2 wt%) binder and DI water were mixed and stirred at 650 rpm for 1 h. The mixture was left to gelate in an ice bath overnight. The isopropanol (2 wt%) and the Ni/Al_2O_3 catalyst (20-45 μm, 17.7 wt%) were added to the mixture and stirred at 850 ml for 30 min (Figure 3-1).

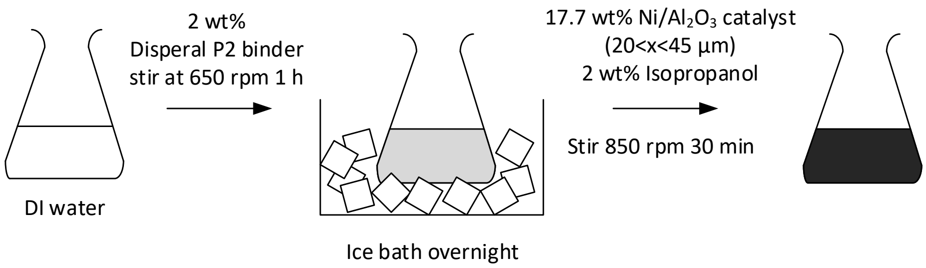

Figure 3-1 Preparation of water and isopropanol-based slurry.

Polyvinyl alcohol (PVA) based slurries

Polyvinyl alcohol (PVA) was also added to suspend the catalyst particles in the slurry. In addition, 0.4 wt% nitric acid (HNO_3) was used to promote the fragmentation of the Disperal P2 binder. PVA based slurries were prepared with different solid to liquid and catalyst to binder ratios as summarized in Table 3-1. PVA based slurries were prepared by adding Disperal P2 binder (1.65 or 2.0 wt% with size 20 < x < 45 µm) to a 0.4 wt% HNO_3 solution under continuous stirring for 30 min at 400 rpm. After 48 h, PVA (5.2 or 5.0 wt%) and a Ni/Al_2O_3 catalyst (12.1 or 14.0 wt%) were added and then stirred for 2 h at 600 rpm. Afterwards, the slurry was left to rest for at least 4 days to allow for it to gelate (Figure 3-2). Prior to dip-coating the slurry was re-stirred.

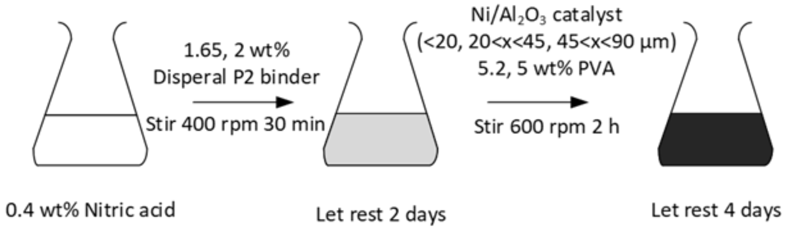

Figure 3-2 Preparation of PVA based slurry.

A slurry with a low solid to liquid ratio (0.5:5.0) and a high catalyst to binder ratio (9:1) was prepared as depicted in Figure 3-3. The slurry was sonicated for 1 h in order to facilitate the disaggregation of the binder and the catalyst particles. Afterwards, the slurry was again stirred and then left to rest until it had thickened (its viscosity increased).

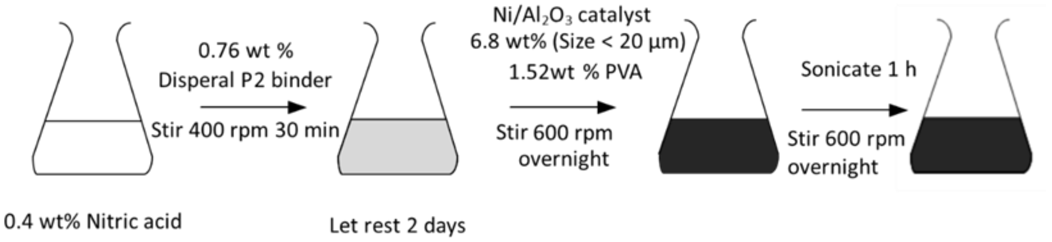

Figure 3-3 Preparation of slurry 6, a low solid content PVA based slurry.

3.2.2.3 Preparation of slurry for two-step coating slurry

A two-step coating approach in which the plate was coated first with a binder and then with a catalyst was investigated. It was hypothesized that the binder layer would help with catalyst particle adhesion.

As shown in Figure 3-4, the binder slurry was prepared by adding the binder (2 wt%) into a 0.4 wt % HNO_3 solution while stirring at 400 rpm for 30 min. After 48 h, PVA (4 wt %) was added and the mixture was stirred at 600 rpm for an additional 2 h.

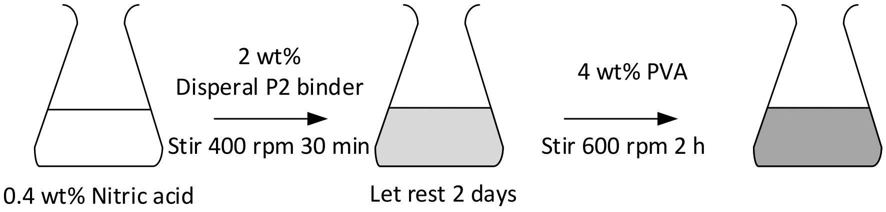

Figure 3-4 Preparation of slurry 7, binder slurry.

The catalyst slurry was prepared by adding 4.3 g of catalyst (45<x<90 µm) and 1.55 g of PVA to 25 g of DI water while it was stirred at 600 rpm for 2 h (Figure 3-5).

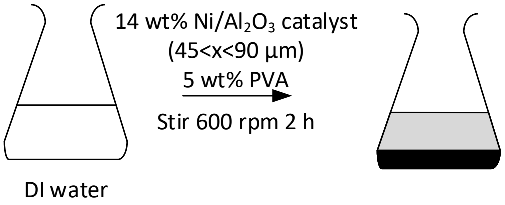

Figure 3-5 Preparation of slurry 8 without Disperal P2 binder slurry.

Table 3-1 summarizes all of the prepared slurries and their components. Six catalyst slurries were prepared for one-step coating experiments. The first prepared slurry was an isopropanol-based catalyst slurry while the second slurry was prepared for testing the used of polyvinyl alcohol (PVA). Slurries #3-5 were prepared from catalysts with different particle diameters (d_P) to investigate the effect of particle size on the catalyst loading. The sixth slurry was prepared with the lowest solid to liquid ratio. Slurries #7 and 8 were used for two-step coating.

Table 3-1 Components of catalyst slurries.

no.	Solvent	Disperal [wt%]	Ni/Al_2O_3 [wt%]	d_P [µm]	PVA [wt%]	Solid : Liquid	Catalyst : Binder
One-step coating slurry							
1	DI water + Iso	2.0	17.7	20<x<45	-	1.0 : 5.0	9.0 : 1.0
2	0.4 wt% HNO_3	1.65	12.1	<20	5.2	1.1 : 5.0	7.3 : 1.0
3	0.4 wt% HNO_3	2.0	14.0	<20	5.0	1.3 : 5.0	7.0 : 1.0
4	0.4 wt% HNO_3	2.0	14.0	20<x<45	5.0	1.3 : 5.0	7.0 : 1.0
5	0.4 wt% HNO_3	2.0	14.0	45<x<90	5.0	1.3 : 5.0	7.0 : 1.0
6	0.4 wt% HNO_3	0.76	6.8	<20	1.5	0.5 : 5.0	9.0 : 1.0
Two-step coating slurry							
7	0.4 wt% HNO_3	2.0	-	-	4.0	0.3 : 5.0	0.0 : 1.0
8	DI water	-	14.0	45<x<90	5.0	1.2 : 5.0	7.0 : 0.0

3.2.3 Dip-coating

Dip-coating involves the immersion of pre-treated plates into a catalyst slurry as depicted in Figure 3-6. After being weighed, the pre-treated plates were covered with parafilm while leaving only a specific area uncovered on one side. An area of 5 cm^2 was left uncovered for the small plates (2 x 4 cm) while 24 cm^2 was remained uncovered for the large plates (4 x 10 cm). The plates were immersed in the slurry for 1 min before being pulled out at a predetermined speed (50 or 100 mm min^{-1}) equal to its immersion speed. The plates were then hung above the slurry for 1 minute to allow for excess slurry to drip from the plates and were subsequently air dried.

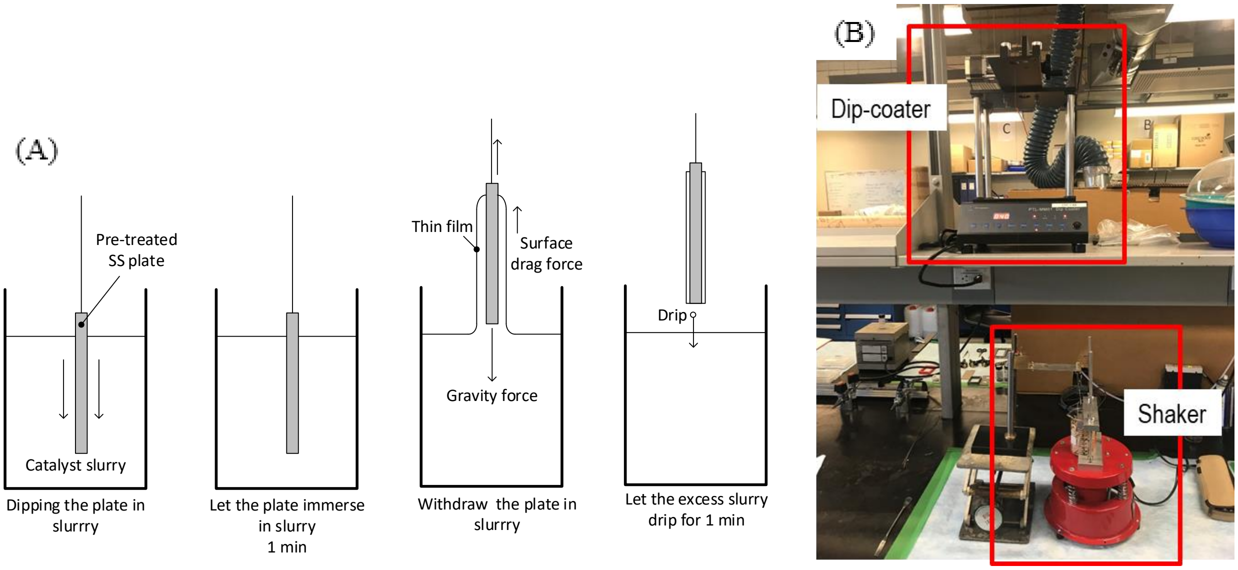

Figure 3-6 (A) Dip-coating process and (B) dip-coating station.

3.2.4 Post-treatment calcination

After each plate was coated, air dried, and its parafilm was removed, it was weighed and then calcined again in a muffled furnace at 300°C for 90 min for post-treatment. After calcination, the plate was reweighed to determine the final solid and catalyst loading values. The latter depended on the catalyst to binder ratio.

3.3 Catalyst and coating characterization

The catalysts, slurry and coated plates were characterized using multiple techniques to determine their respective nickel content, morphology, surface area and catalyst mass distribution. Moreover, a second commercial catalyst (same manufacture) with a nickel content greater than 34 wt% was used and characterized for comparison purposes.

3.3.1 Viscosity

Slurry viscosity was measured using a DV-I+ Brookfield viscometer with a S31 spindle. Approximately 10 ml samples of each slurry were placed in metal containers into which the spindle was submerged. The spindle was set to rotate at 60 rpm after which the viscosity of the sample was calculated in centipoise (cP). As a comparison, 1 cP (1 mPa s) corresponds to the viscosity of water, while honey has a viscosity of 5,000 to 10,000 cP.

3.3.2 Atomic absorption spectroscopy (AAS)

The nickel concentrations present in the slurry and the catalysts were determined using atomic absorption spectroscopy (Varian AA 240 FS). Ni content in the samples was determined by measuring the absorption of light from a cathode lamp at a wavelength specific to Ni. Excited Ni atoms emit energy at a wavelength that can be used to measure the Ni composition of each sample. Prior to the analysis, 100 mg of each catalyst and dried slurry were dissolved in 3 a ml nitric acid solution (67 wt%, Fisher Scientific) and diluted with DI water (total volume 50 ml). Subsequently, 0.01 ml of the sample solution was further diluted with DI water (total volume 14 ml).

3.3.3 N_2 adsorption/desorption

The total surface areas of the catalyst slurry and the catalysts were analyzed via N_2 adsorption/desorption at -196°C. Prior to the analysis, the slurry was dried and calcined at 300°C for 90 min (i.e., representing catalyst coating). Catalyst and slurry samples were degassed under vacuum at 200°C for 16 h.

The measurements were conducted using a Micromeritics Tristar 3000 and based on the principals of the Brunauer-Emmett-Teller (BET) equation. The BET equation follows the Langmuir isotherm theory which dictates the multilayer physical adsorption pattern of gas molecules at active sites.

Subsequently, each adsorbed gas molecule interacts with neighboring molecules within the layer. The BET theory follows the assumptions that the sample is homogenous, and that no interaction occurs between the gas molecules. Furthermore, the theory assumes that all active sites are filled with infinite layers of absorbed gas molecules once saturation has been achieved.

3.3.4 Scanning electron microscopy and energy-dispersive X-ray spectroscopy

Scanning Electron Microscopy (SEM) analysis was performed to investigate the morphology of the catalyst coating on the stainless steel plates. The analysis was done using a FEI Inspect F-50 field emission scanning electron microscope. Moreover, Energy Dispersive X-ray Spectroscopy (EDX) was also performed to investigate the elemental distribution of the catalyst coatings.

3.3.5 Temperature programmed reduction

Temperature programmed reduction (H_2-TPR) was conducted to determine the reduction temperature of the NiO catalysts and slurry. In commercial catalysts, nickel is present in the form of nickel oxide (NiO) and is not active towards CO2 methanation. Nickel is only active in its elemental form (zero-valent metal). During TPR, the metal catalysts are heated under a reducing atmosphere (H_2) while their water production ($NiO + H_2 \rightarrow Ni + H_2O$) is monitored. Thus, the temperature at which the metal is reduced to a lower oxidation state can be determined. H_2-TPR experiments were performed in a fixed bed reactor setup connected to a mass spectrometer (Hiden Analytical, HPR-20). The setup consisted of calibrated mass flow controllers (Vögtlin, 240 red-y smart series), a gas mixing station, a tube furnace, and a mass spectrometer. The outlet gas line was heated to 180°C to avoid water condensation.

100 mg of each sample was loaded and heated under argon (50 ml_N min^{-1}, 99.999%, Megs) at 200°C for 2 h at a heating rate of 4.5°C min^{-1} to remove any water and leftover alcohol from the slurry. The

temperature was then increased to 950°C while H_2 (10 ml_N min^{-1}, 99.999%, Megs) was introduced into the system and mixed with argon (40 ml_N min^{-1}, 99.999%, Megs). While the temperature rose, the mass spectrometer recorded the mass to charge ratio (m/z = 18) corresponding to H_2O.

3.3.6 H_2-chemisorption analysis

Chemisorption was performed to determine the active surface area, nickel cluster size, and nickel dispersion of the samples. Measurements were carried out in an Autosorb iQ gas sorption (Quantachrome) instrument. A specially made U-shaped quartz tube sample cell was used to hold approximately 100 mg of the dried slurry or catalyst sample. Each sample was first pretreated at 200°C for 1 h. The sample was then reduced for 3 h at its reduction temperature predetermined from H_2-TPR experiments. Lastly, the sample was removed for 1 h and cooled to 40°C. Measurements were taken over a pressure range of 40 to 600 Torr.

3.3.7 X-ray diffraction (XRD)

X-Ray Diffraction (XRD) was used to identify the crystallinity of the catalyst. Analyses were conducted on a Bruker D8 Discovery X-Ray Diffractometer with a two-dimensional VANTEC-500 detector and a CuK_α (λ = 1.54056 Å) radiation source. The tube voltage was 40 kV, the tube current was 20 mA and the scan rate was 5° min^{-1}. A generated x-ray beam was directed towards the sample, hitting different atoms, and then diffracting into various directions depending on the atom type hit. Based on atom intensity, the diffracted beams can be detected to obtain the structure and the crystallinity of the analyzed sample [44].

3.3.8 Profilometry

The height profile of the catalyst coatings was recorded by a Dektak XT Bruker that was equipped with a stylus of diameter 12.5 μm (Figure 3-7). The force applied for the profilometry test was 5 mg to prevent damaging the catalyst coating. The spatial resolution was set to 1 data point per 1 µm in the axial direction and 1 data point every 100 µm in the radial direction. By measuring the catalyst height profile of the metal plate's coated area, the catalyst mass over a given interval and the overall catalyst mass distribution were determined.

Figure 3-7 Dektak XT Bruker profilometry.

3.3.9 Mechanical test

Two types of mechanical tests were conducted: (1) under cold flow conditions and (2) under hot flow conditions. For the former, the plate was placed in a 3D printed channel and then subjected to an Ar flow of 600 ml_N min^{-1} for 1 h. The weight of the plates was recorded before and after the test to determine the amount of catalyst lost.

The hot flow tests were done using a tubular glass reactor embedded in a furnace (Figure 3-8). One stainless steel and 2 Fe-Cr alloy plates of size 2.5 x 10 cm were coated, placed in the glass reactor and heated in Ar (100-430 ml_N min^{-1}) to 400°C for 500 h. Their weight changes were recorded to determine how much catalyst was lost.

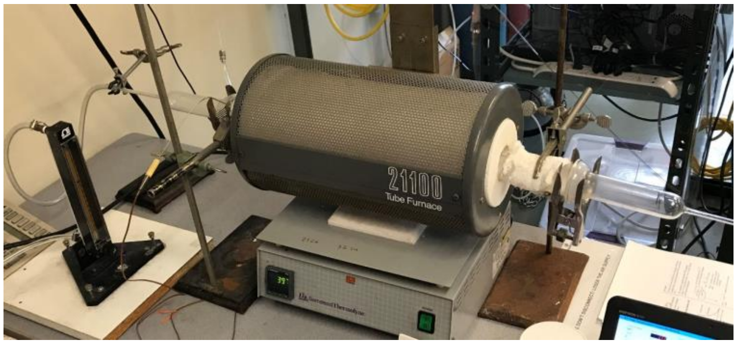

Figure 3-8 Thermolyne 21100 tubular furnace setup.

3.4 Activity measurements

3.4.1 Catalytic plate reactor setup

Reactivity data of the catalyst coating under CO_2 methanation conditions was collected using an optically accessible catalytic plate reactor (CPR) that had been was designed by our group [40],[45]. The reactor allows for the collection of spatially-resolved information on the axial gas composition and the catalyst surface temperature.

The setup and schematics for the CPR reactor are shown in Figures 3-9 and 3-10. The setup includes a gas mixing station, a water saturator, an optically accessible channel reactor, an infrared camera, a movable sampling system and a gas analyzer. Gases (Ar, H_2, CO_2) are fed though calibrated mass flow controllers (Vögtlin, red-y smart series). The gases are mixed and heated before entering the channel reactor. The total pressure of the system can be controlled using a backpressure regulator (Equilibar, LF). The outlet gas was cooled and sent to a fume hood.

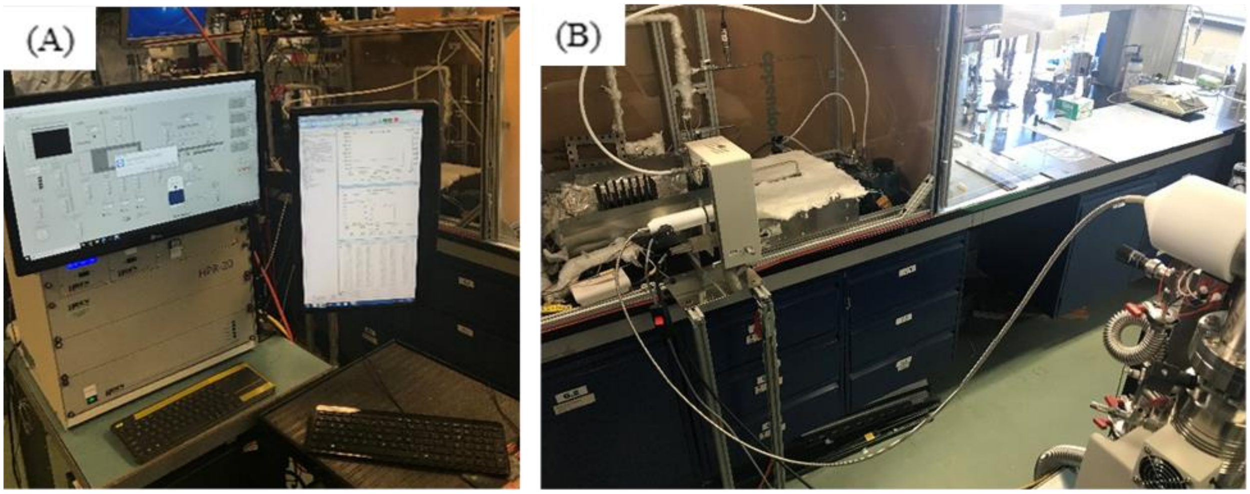

Figure 3-9 (A) Hiden Analytical, HPR-20 mass spectrometer (B) CPR reactor is connected to the MS via capillary.

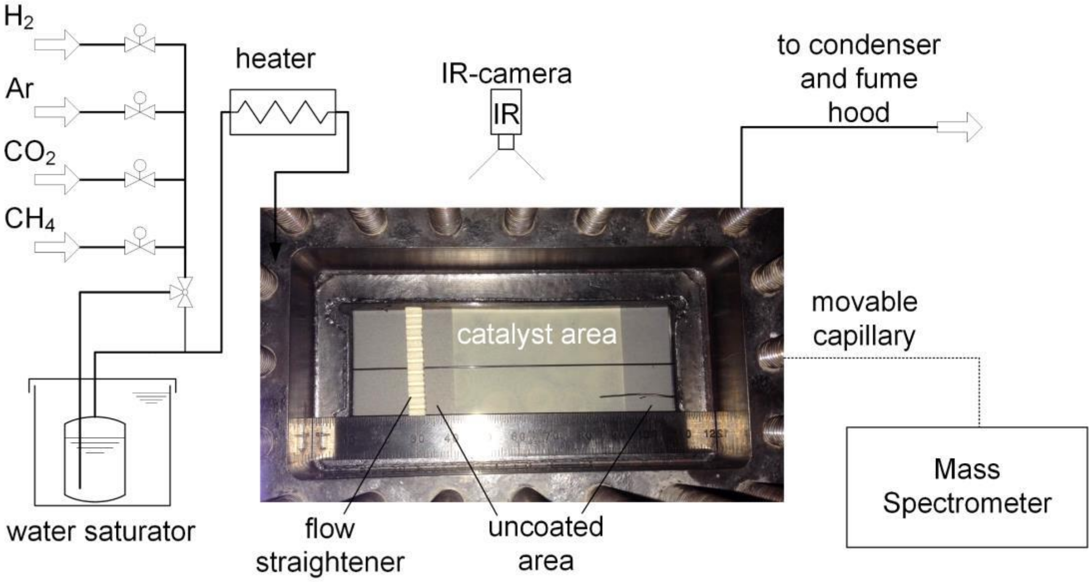

Figure 3-10 Scheme of the catalytic plate reactor test rig [45].

The reactor was made of stainless steel 316L with effective channel dimensions of 40 x 100 x 5 mm. Large 4 x 10 cm coated stainless steel plates were placed on the bottom of the reactor. The chamber was closed with two clear fused quartz glass plates that were designed for optical accessibility and minimization of the intra-channel temperature gradient (Figure 3-11). The quartz glass plates (Heraeus, TSC-3) had a transmissivity of 90% in the 0.2 – 2.0 μm wavelength range. This allowed for the catalyst surface temperature to be observed using a shortwave infrared camera (FLIR, SC2500). The reactor was heated by six heating cartridges distributed under the plate for homogenous heating. High temperature gaskets (Klinger, PMS-AS) were used to separate the glass plates from the stainless steel body of the reactor. The gaskets had a thickness of 1.6 mm and a compressibility factor of 30%. The reactor setup was pressure tested up to 10 bar_{abs} at 600°C. On the side of reactor, a stainless steel capillary with a 0.5 mm outer diameter and a small sampling orifice was inserted into the channel (Figure 3-11). The capillary was moved via a LabView controlled stepper motor and connected to the mass spectrometer.

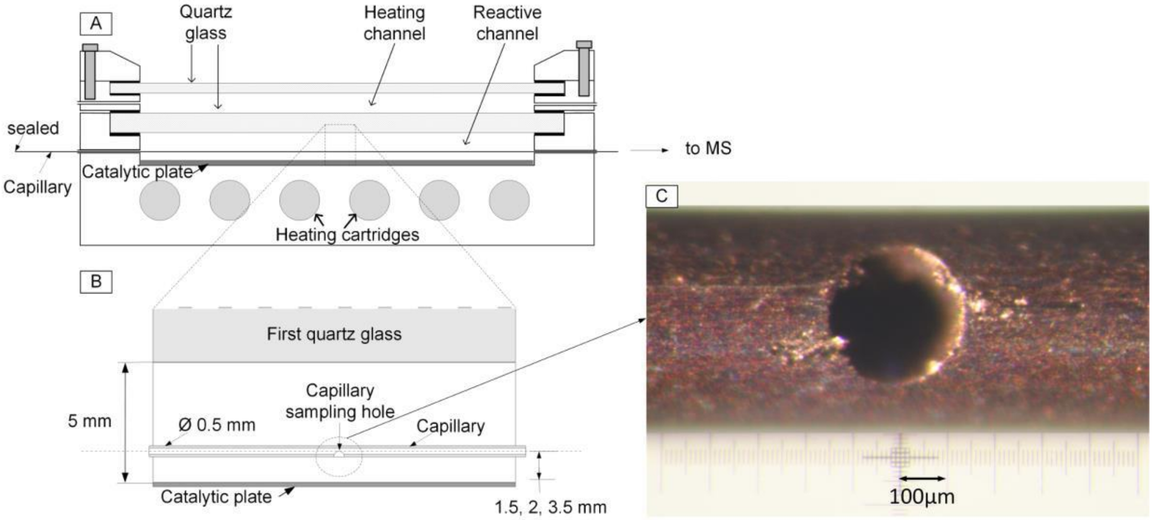

Figure 3-11 Side view scheme of the catalytic plate reactor body, (B) Depiction of capillary going through reactor, (C) Picture of the sampling orifice on the capillary [45].

3.4.2 Experimental procedure

Prior to conducting experiments, the catalyst on the plate was reduced with 50 mol% H_2 (99.999% Megs Specialty Gases) in Ar (99.999% Megs Specialty Gases) for 8 h at a reduction temperature determined from H_2-TPR analysis. The reactor was cooled to 300°C. Then, the sampling orifice of the capillary was moved to the zero position (10 mm before the coated area starts). The reactivity tests were conducted at temperatures between 300 and 400°C at 1.3 bar_{abs} with total volumetric flowrate of 100 ml_N min^{-1} at a fixed H_2/CO_2 mol ratio of 4:1 with Ar as the internal standard. CO_2 (99.995%, Megs Specialty Gases) was fed stepwise until the correct flow rate was achieved.

IR surface and line profiles were recorded before CO_2 was added and throughout the methanation reaction. The sampling capillary was set to move once the concentration of the species at the zero-position reached steady state. The capillary was held for 45 s at each position and continued moving in the direction of the flow towards the end of reactor. For each run, up to 90 data points were collected per gas species.

The gas composition was determined using a calibrated quadrupole mass spectrometer (Hiden Analytical, HPR-20). The mass spectrometer was calibrated specifically to quantify the amounts of H_2 (2 amu), CH_4 (15 amu), H_2O (18 amu), CO (28 amu), 369 Ar (40 amu) and CO_2 (44 amu). Moreover, the fragmentation of CO_2 to CO signal at 28 amu was also considered in the calibration. Ar was again set as the internal standard.

Chapter 4

4 Results and discussions

This section of the thesis presents the results of each experiment and characterization. The results were compared and discussed with respect to the variables established for each experiment.

4.1 Pre-treatment

After the 2 x 4 cm stainless steel plates were pre-treated using the methods described in experimental section, the surface roughness of the plates was measured using profilometry. A picture of an untreated stainless steel plate and its surface roughness are shown in Figure 4-1. The untreated plate had a smooth reflective silver surface with a roughness smaller than 1 ± 0.25 µm.

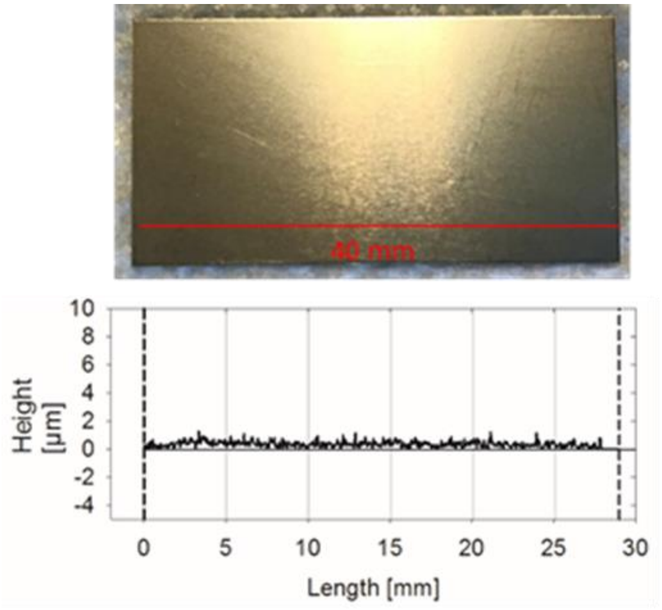

Figure 4-1 Picture and surface roughness of untreated stainless steel plate.

4.1.1 Thermal treatment

After the stainless steel plates were calcined at temperatures of 600-900°C, their physical characteristics changed, most notably their color as shown in Figure 4-2. Stainless steel changes color because an iron oxide layer is formed during calcination. This iron oxide layer interferes with the wavelength of light deflected form the stainless steel surface. Differences in oxide layer thickness are responsible for the different colors of the surface. The plates calcined at 600°C for 30 min turned blue while retaining their reflective surface. However, the surface color of the stainless steel plates became darker and less reflective with increasing calcination temperatures. The plates calcined at 700°C presented a more brownish color with only minor traces of blue shadings. The plates treated at 800°C became entirely brown in color. Lastly, the plates calcined at 900°C were matte and almost blackened. This implies that the whole surface was covered by an oxide layer.

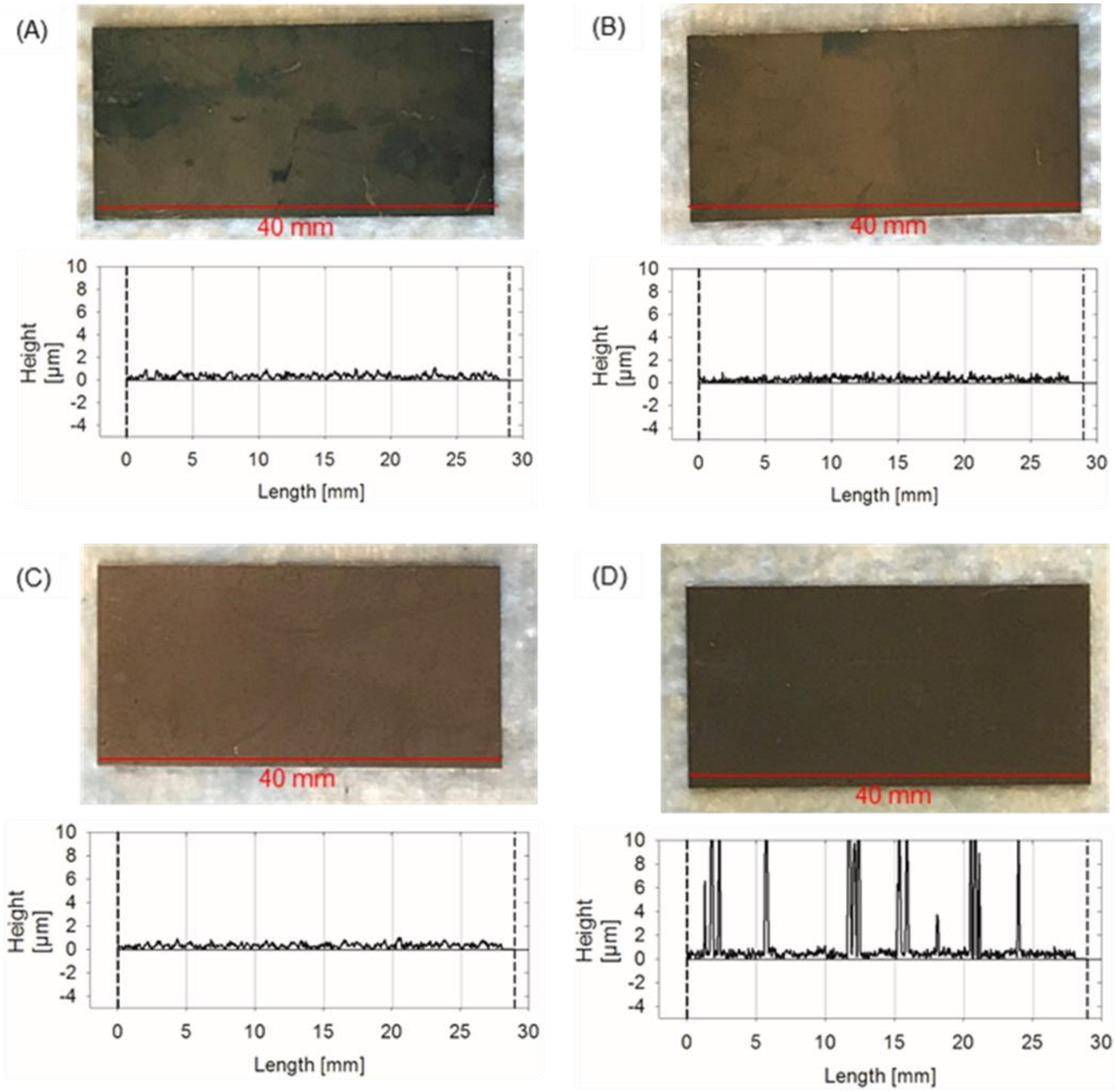

Figure 4-2 Pictures and surface roughness of 30 min thermally treated stainless steel plates: (A) 600°C, (B) 700°C, (C) 800°C, (D) 900°C.

While the color change of the treated plates was noticeable, the surface roughness of the 600-800°C treated plates was not significantly different than the roughness of the untreated plates. The plates treated at 600, 700, and 800°C had a surface roughness of less than 1 µm, which was also the case for untreated plates. On the other hand, the 900°C treated plates' surfaces showed sharp peaks on the measured height profile. While the plates treated at 900°C had a base surface roughness of less than 1 µm, the peaks were measured as more than 10 µm. These nodule peaks were the product of the γ-Fe_2O_3 (Austenite) layer swelling [29]. Although the formation of nodule peaks increased the overall surface roughness of the plates, too few were formed, and they were separated far apart from each other. It was hypothesized that the nodes would not contribute to increasing the adhesion of catalyst particles on the surface.

4.1.2 Chemical treatment

The surface properties of the chemically treated stainless steel plates changed drastically after etching them in an H_2SO_4 solution for 2 h. The plates lost their light reflecting property and became grey in color. Their surface roughness also increased to the point that it could be felt by touch. The roughness measurements obtained from profilometry are shown in Figure 4-3. Stainless steel plates etched in 10 and 20 wt% H_2SO_4 solutions had a surface roughness of approximately 3 µm with differences in height of ± 2 µm. The plates etched in 30 wt% H_2SO_4 solution had a slightly higher surface roughness of 4 µm with some peaks reaching 6 µm with differences in the height profile of ± 2.5 µm. Compared to the thermally treated plates, the chemically treated plates had a greater surface roughness. It is expected that the increased roughness will promote adhesion between the surface and the catalyst coating by allowing the catalyst particles to deposit themselves onto the uneven surface.

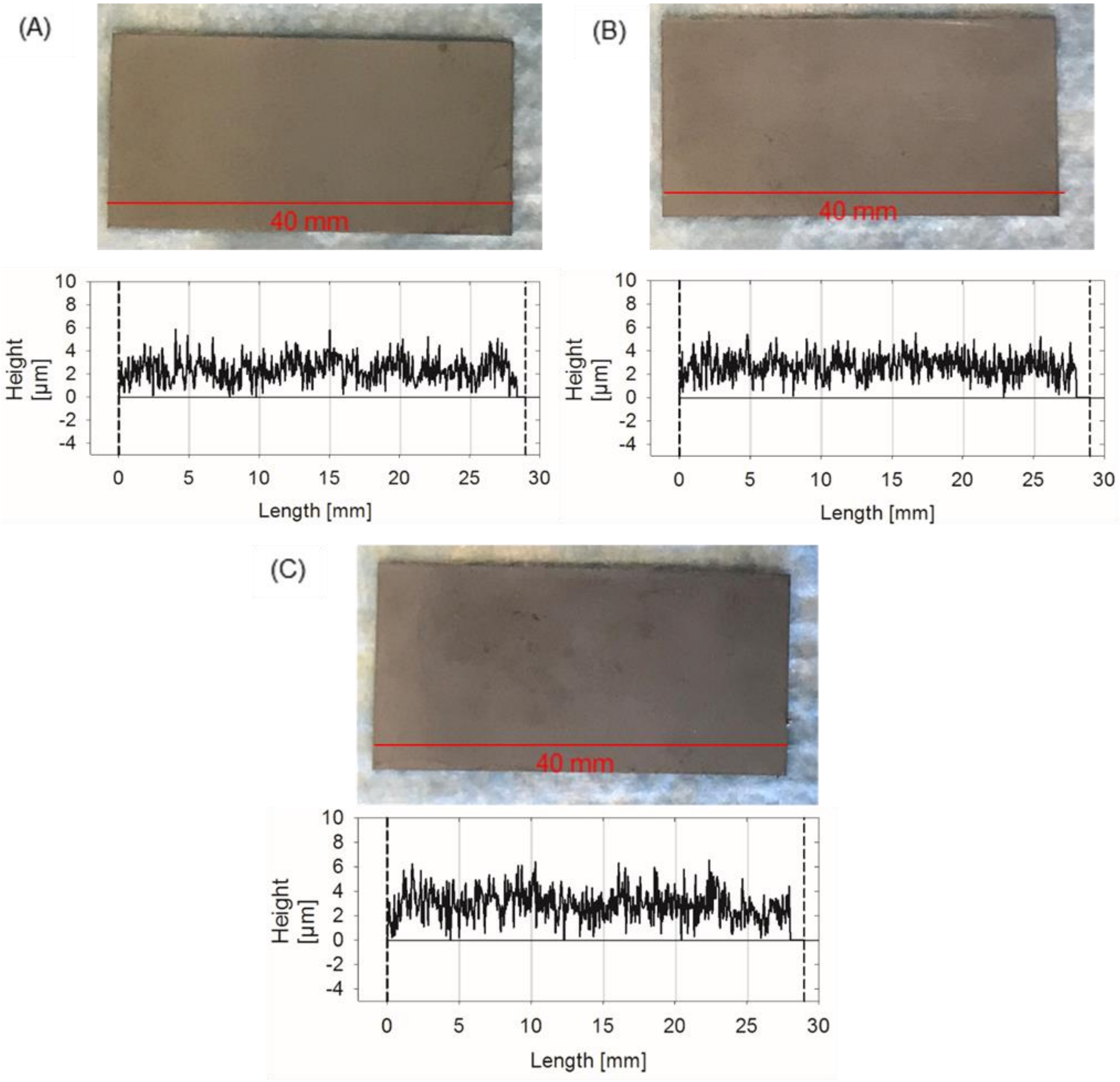

Figure 4-3 Pictures and surface roughness of 2 h chemically treated stainless steel plates: (A) 10 wt. % H_2SO_4, (B) 20 wt% H_2SO_4, (C) 30 wt. % H_2SO_4.

4.1.3 Mechanical treatment

After polishing with 400 grit sandpaper, the mechanically treated plates still retained their silver reflective surface (Figure 4-4). However, scratch marks that had been left by the sandpaper were visible to the naked eye. Although the surface alterations could be visually observed, the measured surface roughness showed no significant changes from the untreated stainless steel plates. The surface roughness of both the perpendicularly and axially polished plates was of approximately 1 μm with height differences of less than ± 0.25 μm. With little to no change in surface roughness, it was not expected that the mechanically treated plates would produce a high catalyst loading.

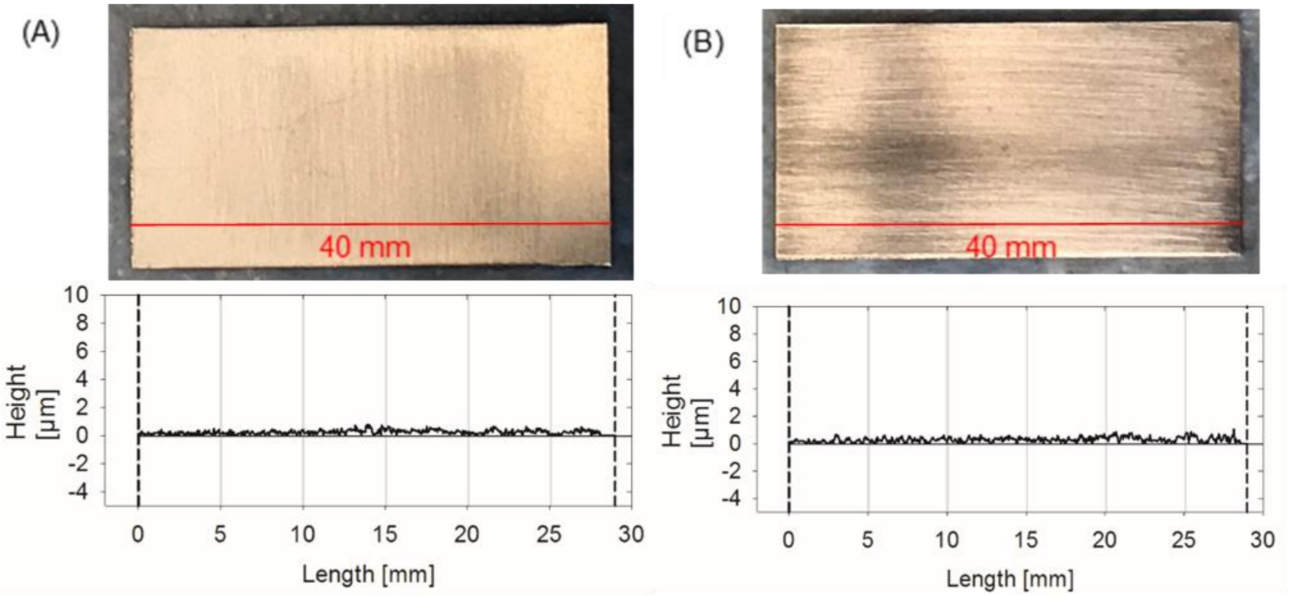

Figure 4-4 Pictures and surface roughness of mechanical treated stainless steel plates: (A) perpendicularly polished, (B) Axially polished.

4.2 Catalyst slurry

4.2.1 Isopropanol based catalyst slurry

Once prepared, the isopropanol-based catalyst slurries would rapidly evaporate. Due to the high evaporation rate of isopropanol in the mixture, the slurry's solvent gradually decreased leaving the catalyst particles to quickly sediment to the bottom of the mixture. The slurry's decreasing liquid to solid ratio led to an increase in its viscosity. Over the span of a week, the solvent of the prepared isopropanol-based slurry dried up entirely, leaving only the dried solid catalyst sediments in the container. Keeping isopropanol-based slurries at low temperatures in a refrigerator can prolong their storage time. However, the aim of this research was for the slurry to be stored at room temperature. Therefore, the slurries were stored in a cabinet. The inconsistency between the viscosities and short storage time of the isopropanol-based slurries made them unsuitable for the coating process and they were henceforth not used in any dip-coating experiments.

4.2.2 Polyvinyl alcohol (PVA) based catalyst

In comparison, catalyst slurries prepared using PVA in a 0.4 wt.% HNO_3 solution had longer storage times than the isopropanol-based slurries. However, they required longer preparation times. Once the PVA and Ni catalysts were added to the mixture, the slurries were left to gel in order to increase and stabilize their viscosity. The gelation process usually took over four days as described in chapter 3.3.2 (Figures 3-2 and 3-3). Once gelated, the slurries can be kept for multiple months in gel form and could always be stirred and used at any time.

4.2.3 Viscosity of slurries

A summary of the measured viscosities of the prepared slurries is reported in Table 4-1. The one step-slurries, #1-5, were very viscous and exceeded the limits of the viscometer's spindle. This indicated that the viscosities must have been greater than 2000 cP. This is because all five of the slurries had a rather high solid to liquid ratio of over 1:5. However, slurry #6, which was prepared with a 0.5 : 1.0 solid to liquid ratio had lower viscosity of 152 cP.

The two-step slurry, binder slurry #7, had a low viscosity of 3.4 cP as it was prepared with a 0.3 : 5.0 solid to liquid ratio and without a catalyst mixture. The catalyst slurry #8 had a low viscosity of 27 cP even though it was prepared with a high solid to liquid content of 1.2 : 5.0. The low viscosity of this slurry was due to the lack of Disperal binder in the mixture. Without the alumina binder, the catalyst particles rapidly sedimented to the bottom of the slurry creating gradient of the viscosity and solid ratio in the slurry.

Table 4-1 Viscosity measurements of prepared slurries.

no.	**Solvent**	**Solid : Liquid [g / ml]**	**Catalyst : Binder [g/g]**	***d_p* [µm]**	**Viscosity [cP]**
One-step coating slurry					
1	DI water + Iso	1.0 : 5.0	9.0 : 1.0	20<x<45	>2000
2	0.4 wt% HNO_3	1.1 : 5.0	7.3 : 1.0	<20	>2000
3	0.4 wt% HNO_3	1.3 : 5.0	7.0 : 1.0	<20	>2000
4	0.4 wt% HNO_3	1.3 : 5.0	7.0 : 1.0	20<x<45	>2000
5	0.4 wt% HNO_3	1.3 : 5.0	7.0 : 1.0	45<x<90	>2000
6	0.4 wt% HNO_3	0.5 : 5.0	9.0 : 1.0	<20	152 ± 1
Two-step coating slurry					
7	0.4 wt% HNO_3	0.3 : 5.0	0.0 : 1.0	-	3.4 ± 0.1
8	DI water	1.2 : 5.0	7.0 : 0.0	45<x<90	27 ± 1

4.3 Catalyst coating

4.3.1 Effect of pre-treatment

The first set of dip-coating experiments was performed using the second slurry, the PVA based slurry with a 1.1 : 5.0 solid to liquid ratio and a 7.3 : 1.0 catalyst to binder ratio (#2 in Once prepared, the isopropanol-based catalyst slurries would rapidly evaporate. Due to the high evaporation rate of isopropanol in the mixture, the slurry's solvent gradually decreased leaving the catalyst particles to quickly sediment to the bottom of the mixture. The slurry's decreasing liquid to solid ratio led to an increase in its viscosity. Over the span of a week, the solvent of the prepared isopropanol-based slurry dried up entirely, leaving only the dried solid catalyst sediments in the container. Keeping isopropanol-based slurries at low temperatures in a refrigerator can prolong their storage time. However, the aim of this research was for the slurry to be stored at room temperature. Therefore, the slurries were stored in a cabinet. The inconsistency between the viscosities and short storage time of the isopropanol-based slurries made them unsuitable for the coating process and they were henceforth not used in any dip-coating experiments.

4.3.2 Polyvinyl alcohol (PVA) based catalyst

In comparison, catalyst slurries prepared using PVA in a 0.4 wt.% HNO3 solution had longer storage times than the isopropanol-based slurries. However, they required longer preparation times. Once the PVA and Ni catalysts were added to the mixture, the slurries were left to gel in order to increase and stabilize their viscosity. The gelation process usually took over four days as described in chapter 3.3.2 (Figures 3-2 and 3-3). Once gelated, the slurries can be kept for multiple months in gel form and could always be stirred and used at any time.

4.3.3 Viscosity of slurries

A summary of the measured viscosities of the prepared slurries is reported in Table 4-1. The one step-slurries, #1-5, were very viscous and exceeded the limits of the viscometer's spindle. This indicated that the viscosities must have been greater than 2000 cP. This is because all five of the slurries had a rather high solid to liquid ratio of over 1:5. However, slurry #6, which was prepared with a 0.5 : 1.0 solid to liquid ratio had lower viscosity of 152 cP.

The two-step slurry, binder slurry #7, had a low viscosity of 3.4 cP as it was prepared with a 0.3 : 5.0 solid to liquid ratio and without a catalyst mixture. The catalyst slurry #8 had a low viscosity of 27 cP even though it was prepared with a high solid to liquid content of 1.2 : 5.0. The low viscosity of this slurry was due to the lack of Disperal binder in the mixture. Without the alumina binder, the catalyst particles rapidly sedimented to the bottom of the slurry creating gradient of the viscosity and solid ratio in the slurry.

Table 4-1). The slurry had a viscosity of more than 2000 cP due to its high solid content. The 2 x 4 cm pre-treated plates were dip-coated using dip/pull speeds of 100 mm min^{-1}. This section of the thesis reports on the catalyst loadings of slurry #2 onto the pre-treated stainless steel plates. The catalyst loadings on the plates were compared in order to investigate the effects of different pre-treatment methods and to determine which method produced the highest loadings. Each experiment was repeated three times to ensure the accuracy of the data.

Averaged catalyst coating loadings on the pre-treated plates are shown in Figure 4-5 (plate #22-48 in Appendix). The blue bars represent the coating loadings right after dip-coating and air-drying. The grey bars show the actual catalyst loadings after post-treatment calcination at 300°C for 90 min.

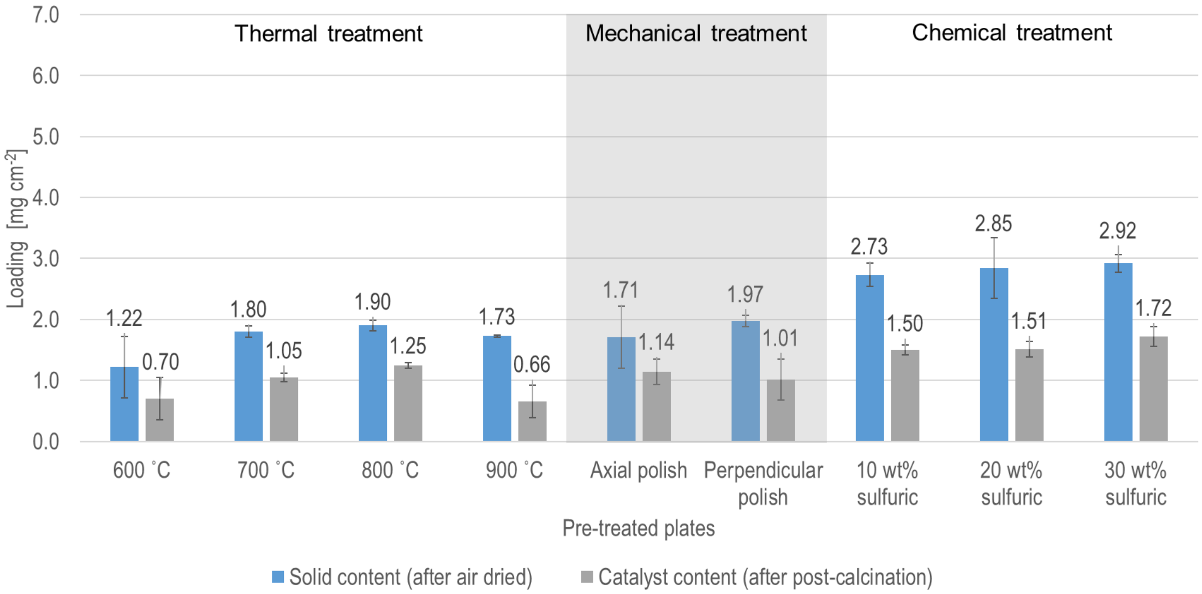

Figure 4-5 Coating loading after air-dried and actual catalyst loading after post-calcination at 300°C on plates with different pre-treatments for slurry #2.

For the thermally treated plates, the catalyst loading increased with increasing pretreatment temperatures from 600 to 800°C (i.e., 0.7 to 1.25 mg cm^{-1}, see Figure 4-5). However, the plates heated to 900°C had a catalyst loading of only 0.66 mg cm^{-2}, the lowest of all the thermally treated plates. At this temperature, the mechanical properties (e.g., hardness, ductility, chemical composition) of AISI 420 stainless steel might change, which would have affected the loading. This is maybe because of swelling of Fe_2O_3 as described in section 4.1.1. These sharp swelled nodes prevented catalyst layer to be formed on the plate properly.

The loadings of the mechanically treated plates were comparable to those of the thermally treated plates. Axially and perpendicularly polished plates had identical catalyst loadings of 1.05 ± 0.20 mg cm^{-2} (Figure 4-5). This indicates that the direction of polishing does not matter.

Chemically treated plates yielded the highest overall coating and catalyst loadings when compared to the thermally and mechanically treated plates. The plates etched with 10 wt% H_2SO_4 had a loading of 1.5 mg cm^{-2}, which increased to 1.7 mg cm^{-2} for the plates pretreated with 30 wt% H_2SO_4 (Figure 4-

5). The high loadings for the chemically treated plates were achieved due to the greater surface roughness of the acid etched plates as seen in Figure 4-3.

The coating height profiles of the plates that produced the highest catalyst loadings for each pre-treatment method are presented in Figure 4-6. All three coatings were homogenous with no uncoated area on the plate. The 800°C treated and axially polished plates both showed similar height profiles of approximately 15 µm. The chemically treated plate which was etched in a 30 wt% HSO$_4$ solution had a greater height profile of approximately 25 µm with several high profile peaks.

Pictures of the catalyst coatings on the thermally treated plates are shown in Figure 4-7 (plate #22-25 in Appendix). The plates calcined at 600-800°C produced even and homogenous catalyst coatings. However, plates calcined at 900°C displayed less homogenous coatings with small uncoated areas. Moreover, it can be observed that the coating was less even than that of the other thermally treated plates.

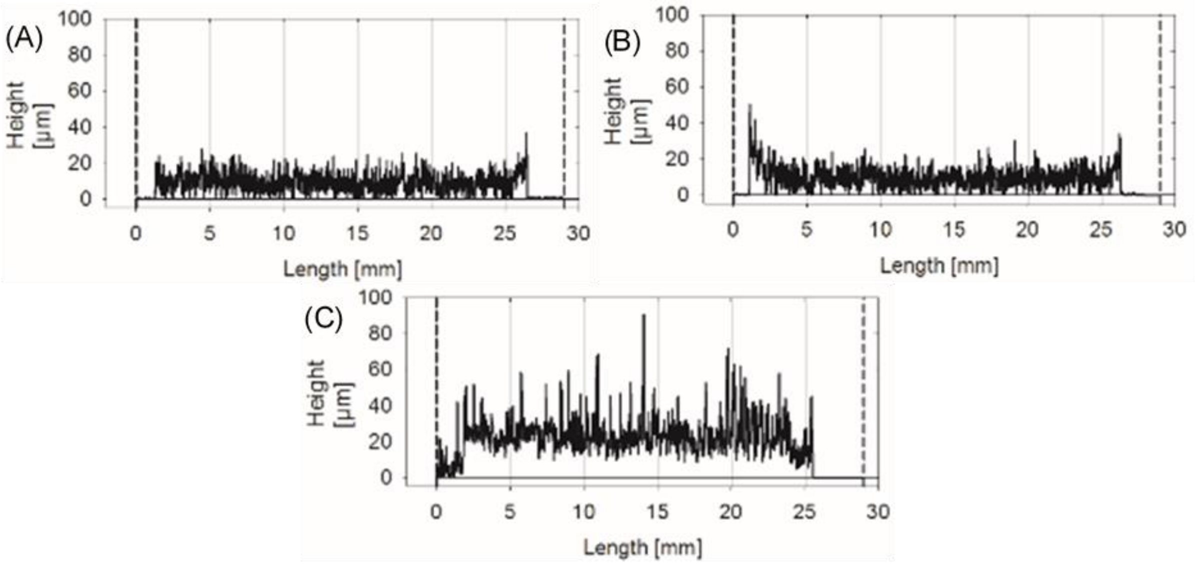

Figure 4-6 Catalyst coating height profile on (A) 800°C treated plate, (B) axially polished plate, nad (C) 30 wt% H$_2$SO$_4$ etched plate.

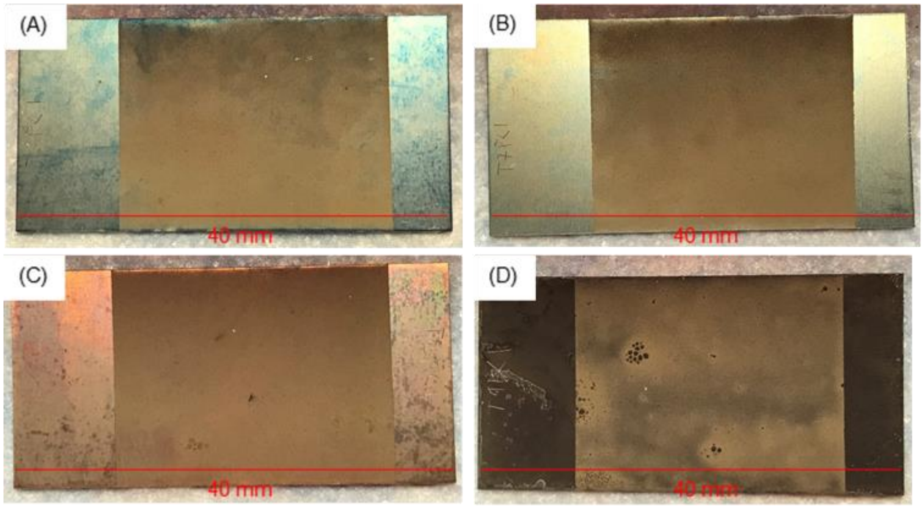

Figure 4-7 Catalyst coating of slurry 2 on thermally treated plate: (A) 600˚C, (B) 700˚C, (C) 800˚C, (D) 900˚C.

Images of the polished plates are presented in Figure 4-8 (plate #26 and #27 in Appendix). Overall, the coatings on the plates were homogenous. However, there were some holes in the coatings on the perpendicularly polished plates. It is worth noting that the plates changed to a reddish-brown color after post-treatment calcination at 300°C. Since the plates were not pre-heated before the experiments, an iron oxide layer formed after post-treatment calcination and changed the plates' color.

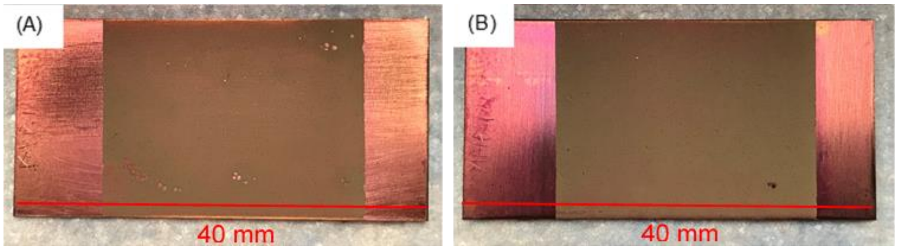

Figure 4-8 Catalyst coating of slurry #2 on mechanically treated plate: (A) Axially polished, (B) perpendicularly polished.

Figure 4-9 depicts the catalyst coatings on the chemically treated plates with different acid concentrations (plate #28, #38, and #39 in Appendix). The stainless steel plates changed to a dark brown color after post-treatment calcination. The thin chromium oxide layer might have been eliminated due to the acid etching. However, this layer could be reformed from the moisture in air. Without the chromium layer present, iron oxide was more rapidly formed during post-treatment calcination than was the case for the thermally and mechanically treated plates. It was also observed that the 30 wt% H_2SO_4 etched plates produced very homogenous coatings while the 10 and 20 wt% H_2SO_4 etched plates had an uneven coating distribution as seen in Figure 4-9.

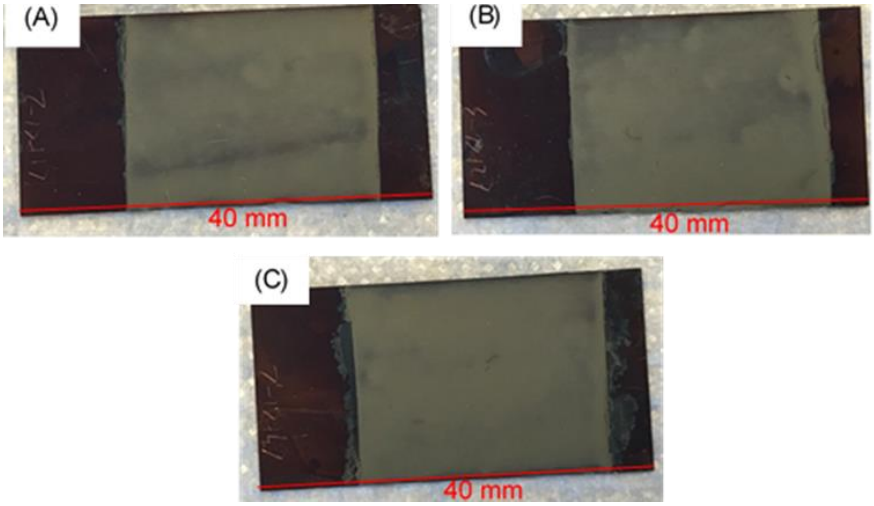

Figure 4-9 Catalyst coating of slurry #2 on chemically treated plate: (A) 10 wt% H_2SO_4 etched, (B) 20 wt% H_2SO_4 etched, (C) 30 wt% H_2SO_4 etched.

4.3.4 Effect of catalyst particle size

The second set of experiments was performed to investigate the effect of catalyst particle size on the catalyst loading. In these tests, 30 wt% H_2SO_4 etched plates were used as they had produced the highest catalyst loadings when compared to the other pre-treated plates. Catalyst slurries #3, #4, and #5 (Table 3-1) had the same solid to liquid ratio (1.3 g : 5.0 ml), catalyst to binder weight ratio (7 : 1) and catalyst mass. However, they had different catalyst particle sizes of <20, 20-45 and 45-90 μm, respectively. Following the previous method, the plates were coated with a dip/pull speed of 100 mm min^{-1}, air-dried, post-calcined, and weighed. The loading results are presented in Figure 4-10 (plate #66, #75, #84 in Appendix).

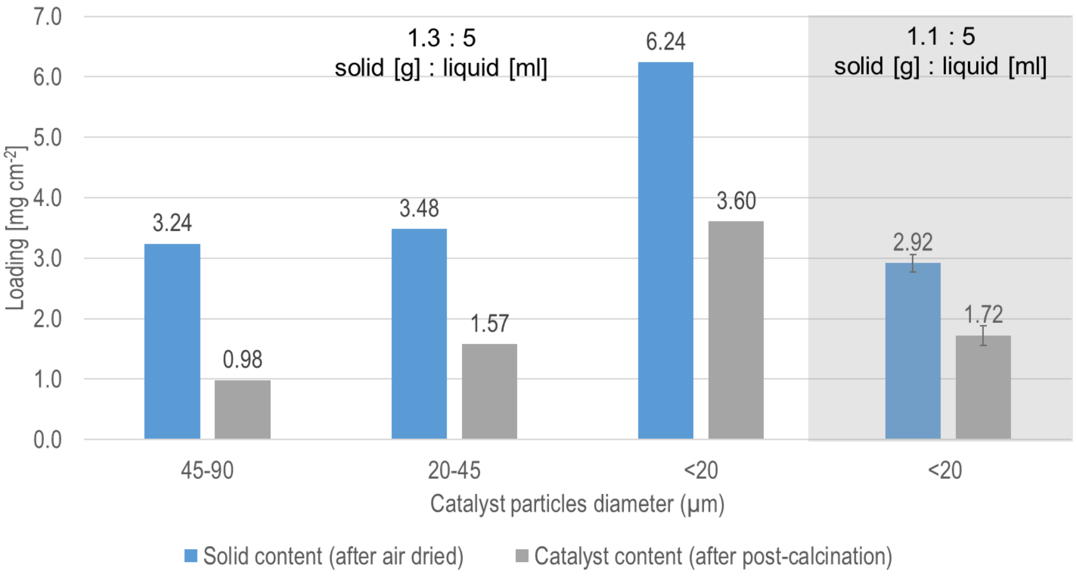

Figure 4-10 Loading of catalyst slurries prepared using different catalyst particle sizes on 30 wt% H_2SO_4 etched plates.

The highest catalyst loading of 3.60 mg cm^{-2} was achieved using the slurry that contained catalyst particles of less than 20 µm (Figure 4-10). With larger particles (20-45 and 45-90 µm), the catalyst loadings decreased to 1.57 and 0.98 mg cm^{-2}, respectively. The catalyst loading for slurry #3 was more than double that of slurry #2, though it was also prepared with catalyst particles of less than 20 µm. The difference between the two slurries was slurry #3's higher solid to liquid ratio of 1.3 : 5.0 compared to the 1.1 : 5.0 ratio of slurry #2.

Even though slurry #5 achieved the highest loading, the coating itself was not homogeneous as depicted in Figure 4-11C. The coating was cracked, most likely due to fast drying. The coatings of slurries #3 and #4 were not homogeneous either (Figure 4-11A and B). The coating produced with a lower solid to liquid ratio (slurry #2) had a smaller catalyst loading but was homogeneous (Figure 4-9C).

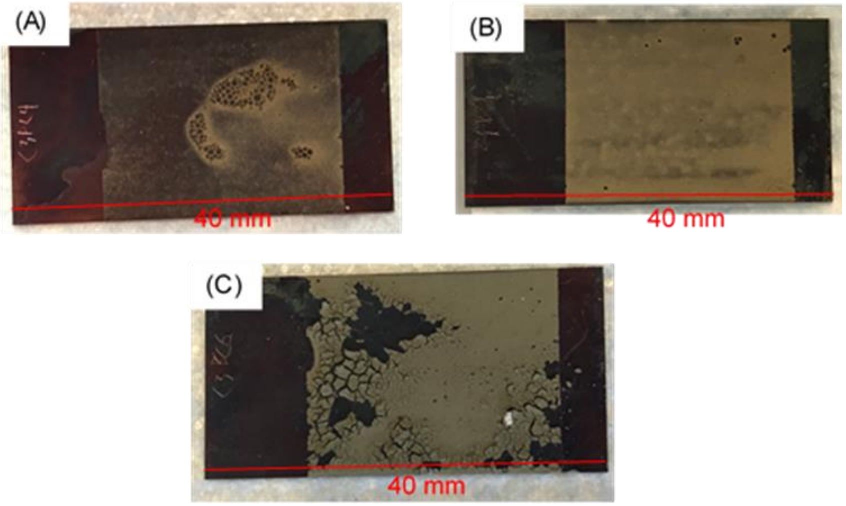

Figure 4-11 Catalyst coating of slurries with solid to liquid content of 1.3 : 5 prepared using different catalyst particles diameter: (A) 40-90 μm, (B) 20-45 μm, (C) < 20 μm (plate #66, #75, #84 in Appendix).

4.3.5 Effect of viscosity and dip/pull speed

It was concluded from the previous experiment that slurries prepared using small catalyst particles of less than 20 μm produced the highest catalyst loadings. However, the high solid to liquid ratio resulted in an uneven and cracked coating. Therefore, further experiments were conducted using slurry #6, which was also prepared using catalyst particles of less than 20 μm. This slurry had a low solid to liquid ratio of 0.5 : 5.0, increased catalyst to binder ratio of 9 : 1 and was sonicated for 1 h. The low solid ratio resulted in a low viscosity of 152 cP as shown in Table 4-1. Stainless steel plates that were treated with 30 wt% H_2SO_4 were dip-coated into the low viscosity slurry with different pull/dip speeds of 50 and 100 mm min^{-1} to study the effect of the coating speed on coating quality.

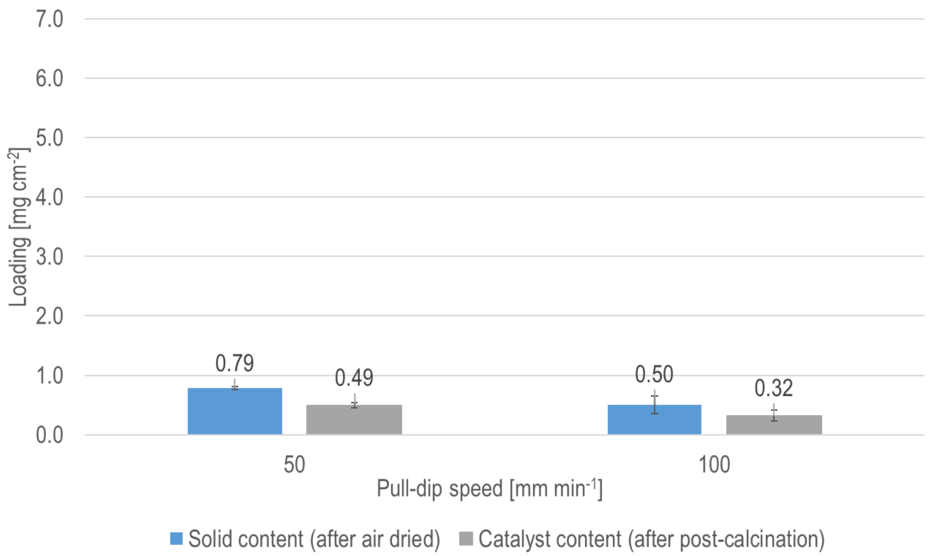

Figure 4-12 Loading of low viscosity catalyst slurry #6 with solid to liquid content of 0.5 : 5 coated with different dip/pull speeds of 50 and 100 mm min^{-1}.

Figure 4-12 shows the averaged coating and catalyst loadings of the low viscosity slurry #6 on the chemically treated plates. Unlike the previous experiment with the high solid content slurry #3, which had a loading of 3.60 mg cm^{-2}, the catalyst loadings of slurry #6 were much lower at only 0.32-0.49 mg cm^{-2}. It was observed that the plates dip-coated at a slower speed of 50 mm min^{-1} (plates #100, #109, and #118 in appendix) yielded higher catalyst loadings of 0.49 mg cm^{-2}, while the plates coated at a higher speed of 100 mm min^{-1} (plate #119-121 in appendix) produced lower catalyst loadings of 0.32 mg cm^{-2}.

The coatings of low viscosity slurry #6 are shown in Figure 4-13. The plate coated with a speed of 50 mm min^{-1} had more solid particles deposited on the surface than the plate coated at 100 mm min^{-1}. While both coatings were homogenous and even, the catalyst coating layers were very thin when compared to the previous coatings achieved using high solid content slurry #3. Therefore, profilometry was not conducted.

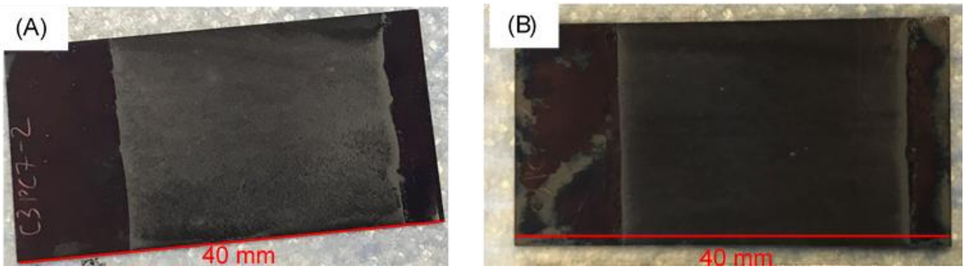

Figure 4-13 Catalyst coating of slurry 6 with solid to liquid content of 0.5 : 5 coated with different speed: (A) 50 mm min^{-1}, and (B) 100 mm min^{-1}.

4.3.6 Multiple coating

After investing the effect of the catalyst particle size, pre-treatment method and pull/dip speed, a desired target catalyst loading was set to be at least 3 mg cm^{-2}. The previous experiment also showed that in order to achieve a homogenous and even coating, the solid to liquid ratio must be lower than 1.3 : 5.0. Unfortunately, slurry #6 with its low solid to liquid ratio of 0.5 g : 5.0 ml and low viscosity of 152 cP yielded a very low catalyst loading of 0.49 mg cm^{-2}.

In order to reach the target catalyst coating of 3 mg cm^{-2}, multiple coatings were needed. In this experiment, a larger chemically treated plate with dimensions of 4x10 cm was used. The plate was dip-coated into slurry #6 with a pull/dip speed of 50 mm min^{-1}. After dip-coating, the plate was air-dried and then dip-coated again. The plate was dip-coated 12 times before post-calcination. A final catalyst loading (plate #89-91 in appendix) of 3.25 mg cm^{-2} was achieved (Figure 4-14).

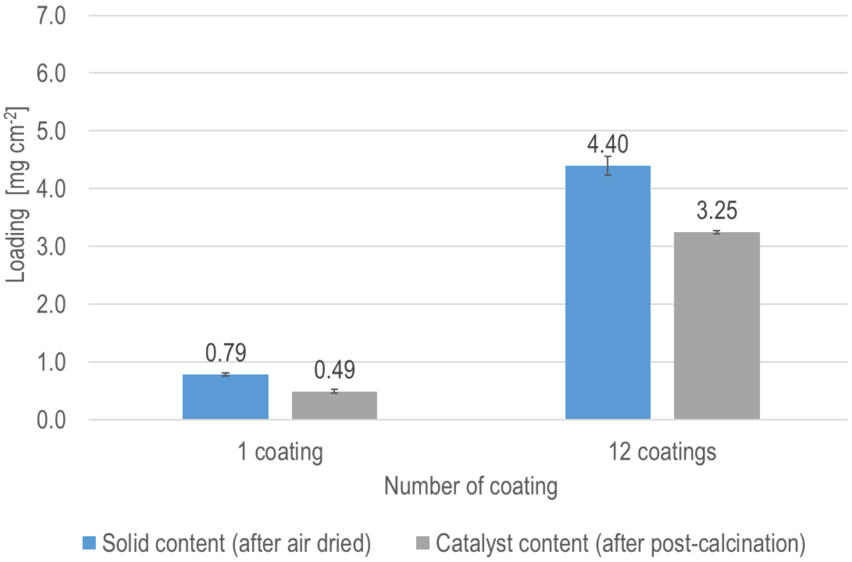

Figure 4-14 Loading of low viscosity catalyst slurry #6 with solid to liquid content of 0.5 : 5 with different number of coatings.

The obtained coating appeared very homogenous with minor cracks at the beginning of the coating (Figure 4-15). Each time the plate was dip-coated, the excess slurry dripped along the length of the plate resulting in an abnormally high loading at the beginning of the coating where the slurry had dripped. During post-calcination, this abnormally high loading caused the coating to crack.

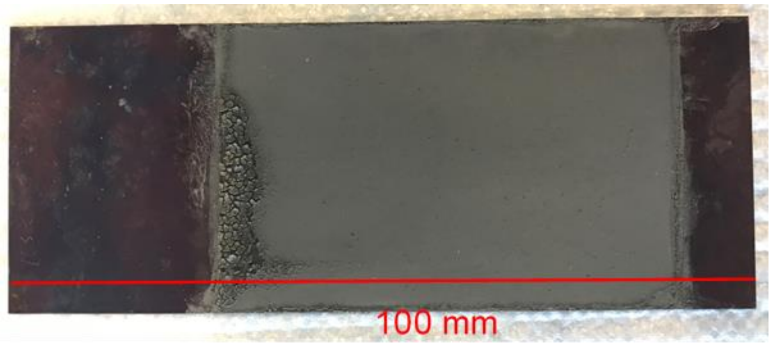

Figure 4-15 Catalyst coating of slurry 6 with solid to liquid content of 0.5 : 5 after 12 dip-coatings.

4.3.7 Mild calcination between coating

Another experiment was conducted to optimize the multiple coating process of the low viscosity catalyst slurry and avoid cracking at the beginning of the coating. Large 4x10 cm stainless steel plates were treated in a 30 wt% H_2SO_4 acid solution and were dip-coated with slurry #6. Two plates were dip-coated 14 times, one of which was air-dried between each coating while the other was calcined in a muffle furnace at a temperature of 100°C for 30 min between each coating. After the plates were dip-coated 14 times, they were post-calcined at 300°C for 90 min.

The two different methods yielded the same results with respect to catalyst loading (Figure 4-16). However, the quality of the coatings was different as illustrated in Figure 4-17. The air-dried plates had cracked slightly at the beginning of the coating, while the mildly calcined plates did not exhibit any signs of cracking.

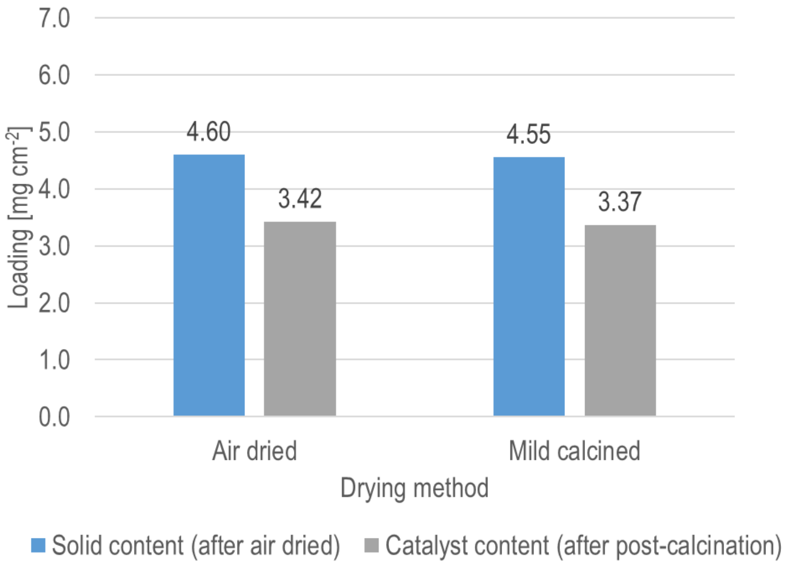

Figure 4-16 Loadings of low viscosity catalyst slurry 6 with 14 coating layers with air-drying and mild calcination between coating.

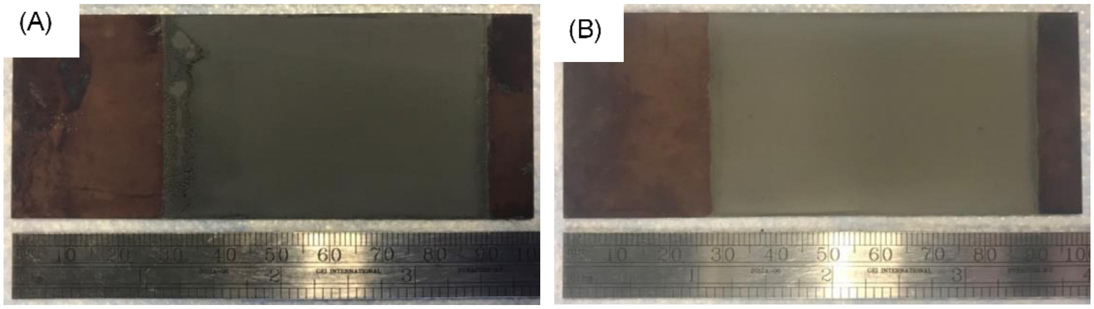

Figure 4-17 Catalyst coating of low viscosity slurry 6 with 14 coating layers with (A) air-drying and (B) mild calcination between coating.

Figures 4-18 and 4-19 depict the differences in the loadings of the air-dried and mildly calcined plates after each dip-coating. It can be seen that the amount of solid retained after each dipping was not constant. It fluctuated significantly for still unknown reasons.

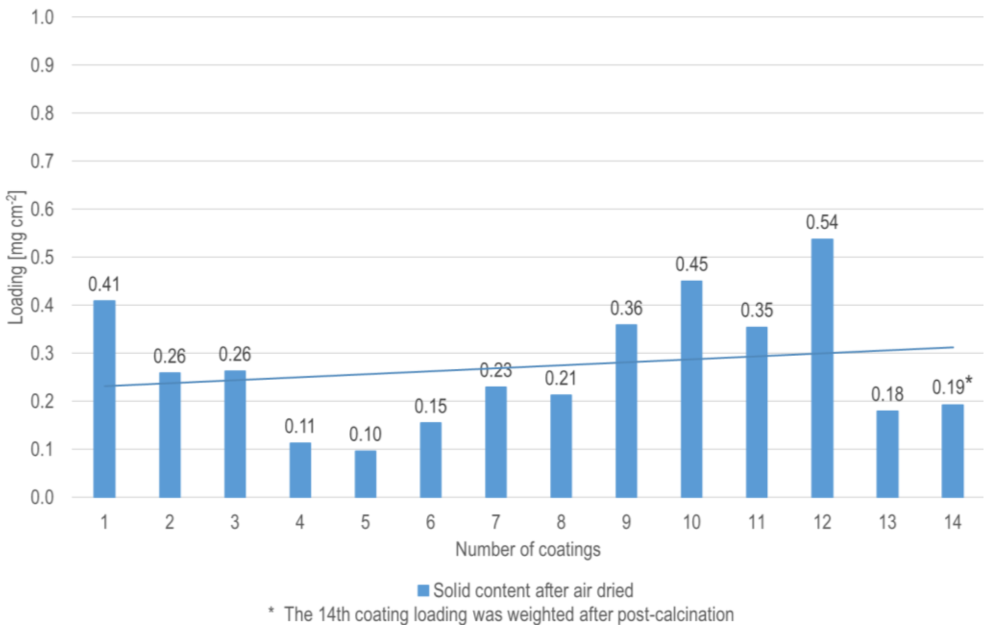

Figure 4-18 Differences in coating loading of slurry 6 on each dip-coating with air drying between coating.

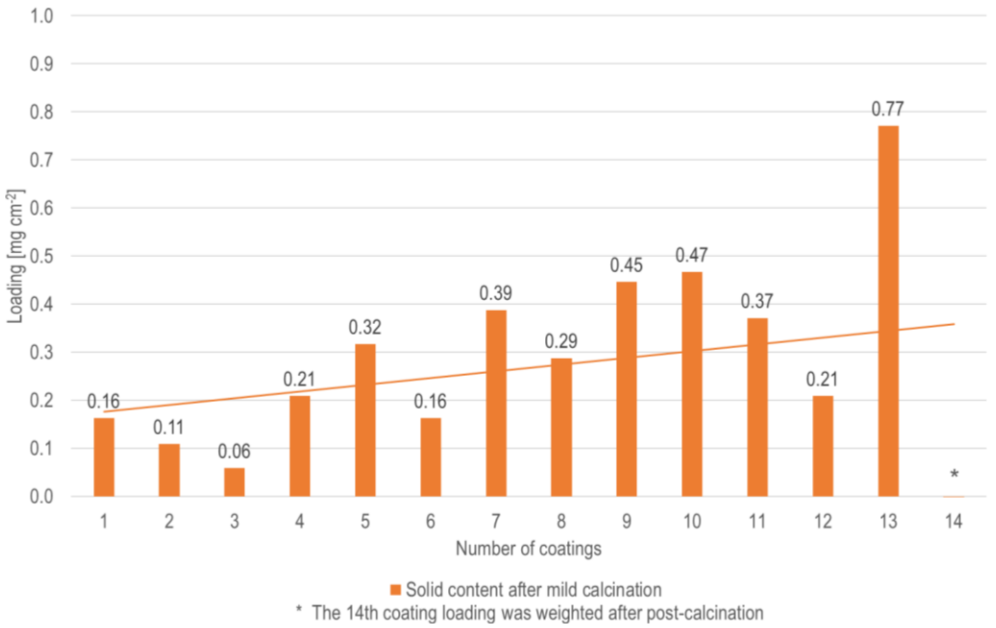

Figure 4-19 Differences in coating loading of slurry 6 on each dip-coating with mild calcination between coating.

4.3.8 2-step coating

An experiment was performed to investigate the 2-step dip-coating method. A chemically treated plate was dip-coated in binder slurry #7 and post-calcined. Then, it was dip-coated for a second time in catalyst slurry #8 and recalcined. It is noted that slurry #7 has binder and PVA without a catalyst component while slurry #8 only contains catalyst and PVA. This was done to investigate whether coating the plates with the binder layer prior to the catalyst layer was better than doing so simultaneously in a one-step coating process. The resulted loadings were compared to those obtained using a 1-step coated plate, which had been coated with catalyst slurry #5. Catalyst slurries #8 and #5 had the same catalyst content of 14 wt%, catalyst diameter of 45-90 μm, and PVA amount of 5.0 wt%.

The loading of the 2-step coated plate (plate # 57 in appendix) is depicted in Figure 4-20. It was shown that the 2-step coated plate had a negligible catalyst loading most likely due to the sedimentation of the catalyst in slurry #8. Without a binder, the solid particles could not be suspended in the slurry.

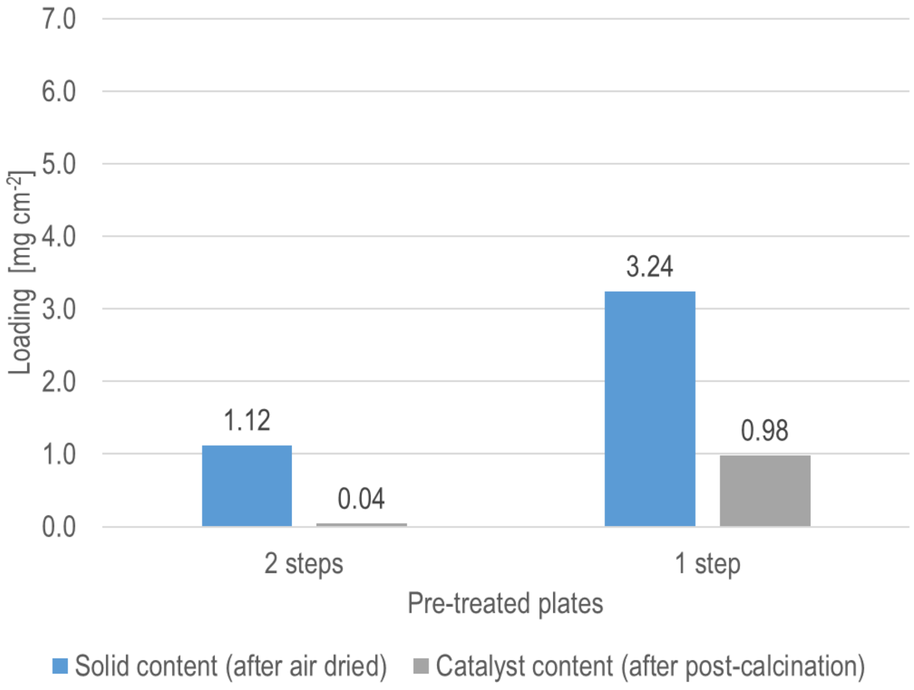

Figure 4-20 Loadings of 2-step coating compared to 1-step coating method.

Figure 4-21 shows the coating obtained using a 2-step coating process. The coating was inhomogeneous and uneven with a high amount of white binder particles deposited at the end of the coating. This was because of the low viscosity of binder slurry #7 (3.4 cP). The binder slurry dripped along the plate very rapidly. Just after the dip-coating of the binder slurry, most of the binder particles had already dripped to the bottom of the plate. After post-calcination, the dripped binder particles remained as a white uneven coating on the plate. Moreover, once the binder coated plate was dip-coated into catalyst slurry #8, the catalyst particles stayed sedimented on the bottom of the slurry even with the use of a shaker. This resulted in a low catalyst deposition on the binder layer.

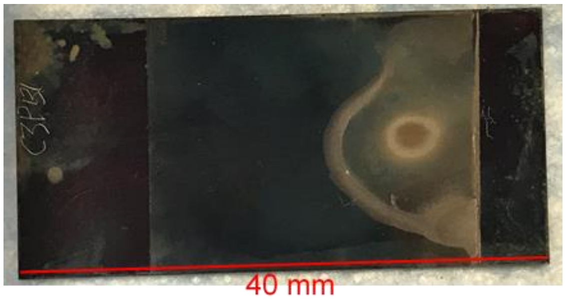

Figure 4-21 Catalyst coating of 2-step coating with binder slurry 7 and catalyst slurry 8.

4.4 Catalyst and coating characterization

4.4.1 Catalyst properties

The Ni content and H_2-chemisorption results of the calcined slurry #6 as well as for the catalysts 1 and 2 are reported in Table 4-2. Catalyst 1 and 2 had a Ni content of 19.0 and 37.7 wt%, respectively. Slurry #6 (prepared with catalyst 1) had a Ni content of 16.5 wt%, which was to be expected due to its high catalyst to binder ratio of 9:1.

Catalyst 1 and its corresponding slurry (#6) had very similar H_2-uptakes and active nickel surface areas of 60-62 µmol g^{-1} and 4.7-4.8 m^2 g^{-1} (Table 4-2) respectively. It is assumed that the binder itself did not have any H_2 uptake. Since catalyst 2 catalyst had the highest Ni content (>34 wt%) it also had the greatest H_2-uptake of 145.7 μmol g^{-1} and active nickel surface area of 11.4 m^2 g^{-1}.

Table 4-2 Ni content and chemisorption results of calcined slurry 6, catalysts 1 and 2.

Sample	**Ni content [wt%]**	**H_2-uptake [μmol g_{solid}^{-1}]**	**Active surface area [m^2 g_{solid}^{-1}]**	**Crystal size [nm]**	**Metal dispersion [%]**
Slurry #6*	16.5 ± 0.6	61.6 ± 1.7	4.8 ± 0.1	11.5 ± 0.3	4.4 ± 0.1
Catalyst 1	19.0 ± 1.3	59.8 ± 0.1	4.7 ± 0.1	13.7 ± 0.1	3.7 ± 0.1
Catalyst 2	37.7 ± 0.8	145.7 ± 5.2	11.4 ± 0.5	11.2 ± 0.5	4.5 ± 0.2

* Slurry #6 was prepared with catalyst 1

N_2 adsorption/desorption

The N_2 adsorption/desorption isotherms and pore size distribution of slurry #6 as well as catalysts 1 and 2 are shown in Figure 4-22.

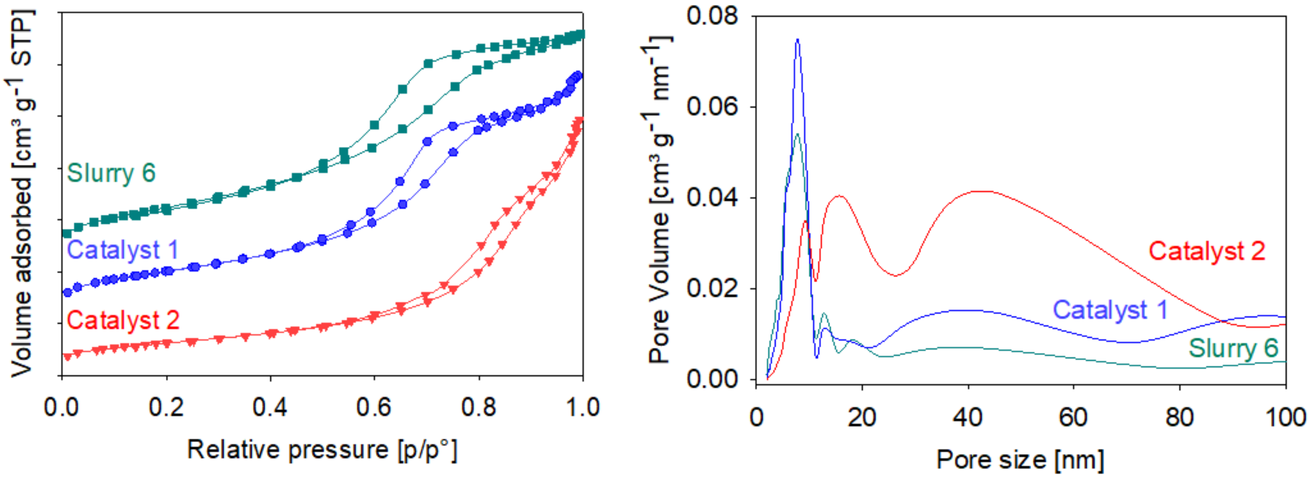

Figure 4-22 (A) N_2 adsorption/desorption isotherm, (B) pore size distribution of calcined slurry #6, catalyst 1 and 2.

According to IUPAC classifications, all three samples have type IV isotherms which are indicative of IV mesoporous materials [46]. However, much like the nature of the catalyst samples, the shapes of the loops differ. The isotherm of calcined slurry 6 contained an H1- type hysteresis loop, which implies the presence of very uniform spherical particles and a cylindrical pore geometry. The commercial catalysts 1 and 2 had isotherms which contained an H4 hysteresis loop, indicating the presence of aggregates of plate-like particles with irregularly shaped pores [46].

Table 4-3 shows the BET surface area results of calcined slurry #6 along with those of the catalysts 1 and 2. Calcined slurry #6 had the highest surface area (216 $m^2 g^{-1}$) amongst the three samples, while the catalyst 1 and 2 had surface areas of 176 and 102 $m^2 g^{-1}$, respectively. The total surface area of slurry #6 was considerably larger than that of catalyst 1. This was the case because the slurry contained a binder that provided additional surface area. In addition, due to sonication of the catalyst slurry the catalyst particle size was further reduced.

Table 4-3 BET surface area analysis of calcined slurry #6, catalysts 1 and 2.

Sample	**BET surface area [$m^2 g^{-1}$]**	**Pore volume [$cm^3 g^{-1}$]**
Slurry #6*	216 ± 19	0.34 ± 0.03
Catalyst 1	176 ± 10	0.33 ± 0.02
Catalyst 2	102 ± 10	0.30 ± 0.03

* Slurry #6 was prepared with catalyst 1

XRD analysis

Figure 4-23 shows the XRD pattern of the plate coated with slurry #6, and the two catalysts. Reference patterns of an Fe-Cr alloy, $NiAl_2O_4$, NiO and γ-Al_2O_3 are also shown for comparison and were taken from the International Centre for Diffraction Data (ICDD) with powder diffraction files (PDF) #054-0387, #010-0339, #044-1159 and #050-074, respectively.

Both catalysts showed diffractions peaks at $2\theta = 44.4°$, corresponding to NiO. Moreover, both catalysts also showed small peaks at $2\theta = 37.2°$ and $2\theta = 66.9°$ which are due to the presence of alumina (γ-Al_2O_3) in the catalysts. However, the intensity of the $2\theta = 44.43°$ peak was higher in the case of catalyst 2 as it had a greater Ni content of more than 34 %. The catalyst coating also displayed signals from NiO and γ-Al_2O_3 but with a lesser intensity. At $2\theta = 43.2°$, the NiO signal peak was much smaller than those of the two catalysts. However, at $2\theta = 44.6°$, 64.8°, and 82.2°, the coating showed strong signal peaks of Fecralloy was present in the stainless steel substrate plates.

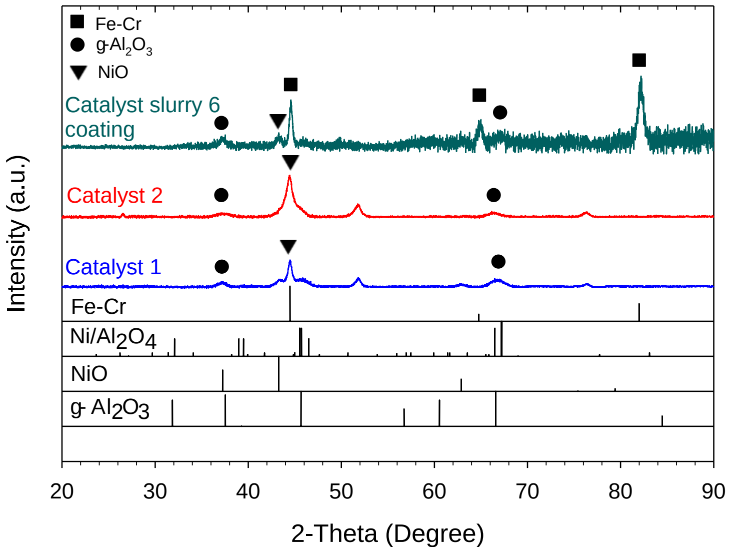

Figure 4-23 XRD analysis of slurry #6 coating, catalysts 1 and 2.

H_2 -TPR profile

The H_2-temperature reduction profiles of slurry #6 along with the catalyst 1 (18 % Ni) and catalyst 2 (>34 % Ni) are shown in Figure 4-24. Catalyst 1, which was used in the preparation of the catalyst slurries showed a water signal peak at 450°C, while catalyst 2 showed a very broad reduction peak at 550°C. For slurry #6, two peaks were visible at temperatures of 300°C and 450°C. From the catalyst 1 profile, it can be deduced that the Ni reducing temperature of the calcined slurry must be 450°C as this catalyst was used to prepare the slurry. The slurry peak at 300°C was due to alcohol and impurities that had been left behind after post-treatment calcination.

The TPR profiles provided the reducing temperature of each catalyst and slurry. Slurry #6 and catalyst 1 can be reduced at 450°C, which is still in the range that the CPR reactor can achieve. However, the high Ni content catalyst 2 needed a higher temperature of 550°C to be reduced which is not possible using the research group's CPR reactor.

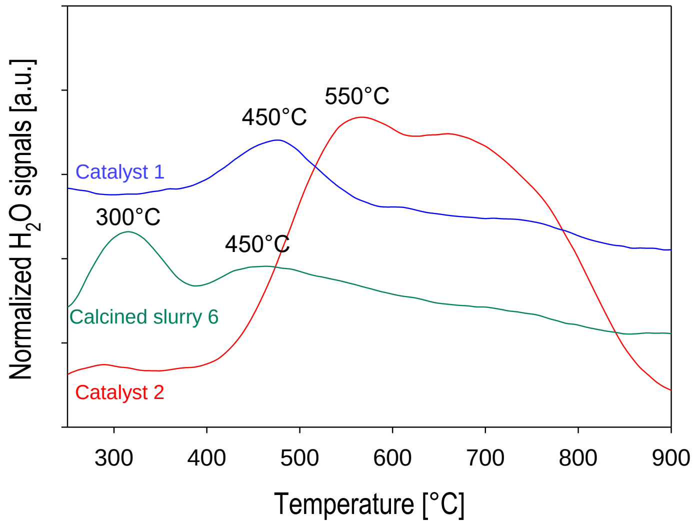

Figure 4-24 H_2-TPR profiles of calcined slurry #6, catalyst 1 (>18 % Ni), and catalyst 2 (>34 % Ni).

SEM and EDX analysis

Figure 4-25 shows the SEM images of the catalyst coated plates. The chemically treated plate was dip-coated in slurry #6 twelve times before post-calcination (plate #90 in the appendix). The plate was air-dried between each coating. The middle of the coating, the area of the coating that appeared the most even and homogenous when viewed by the naked eye, can be seen in the SEM image. However, the SEM images showed that the coating had cracked and that small particles (2-10 µm) had agglomerated to form larger clusters of 50-120 µm. The coating was very dense with the particles packed closely together and separated by crack patterns.

The elemental mapping of EDX images are depicted in Figure 4-26. The images show uniform mappings of each element in the Ni/Al_2O_3 catalyst coating. O, Ni, and Al mappings were homogenous and evenly distributed, though the absence of these elements can be observed in the cracks of the coating.

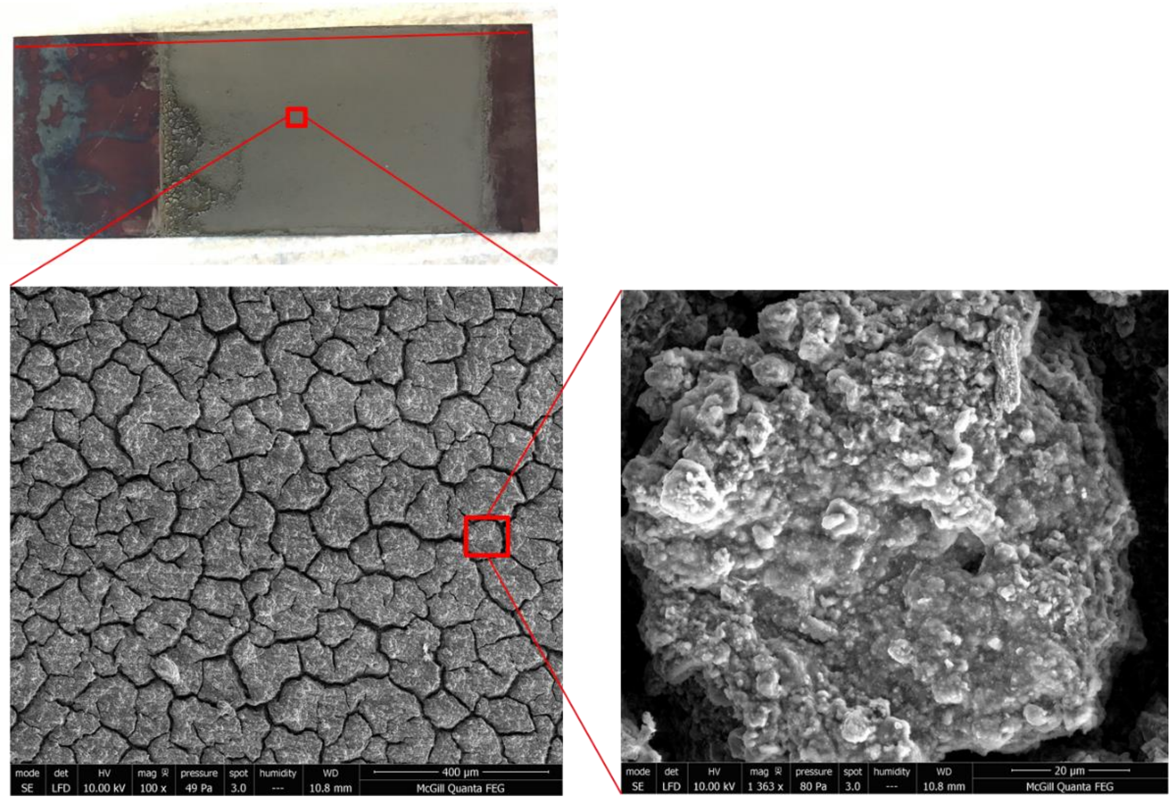

Figure 4-25 (A) Picture of a catalyst coated by slurry #6 stainless steel plate (100 x 40 mm), (B) and (C) SEM image of the coated areas of the plate.

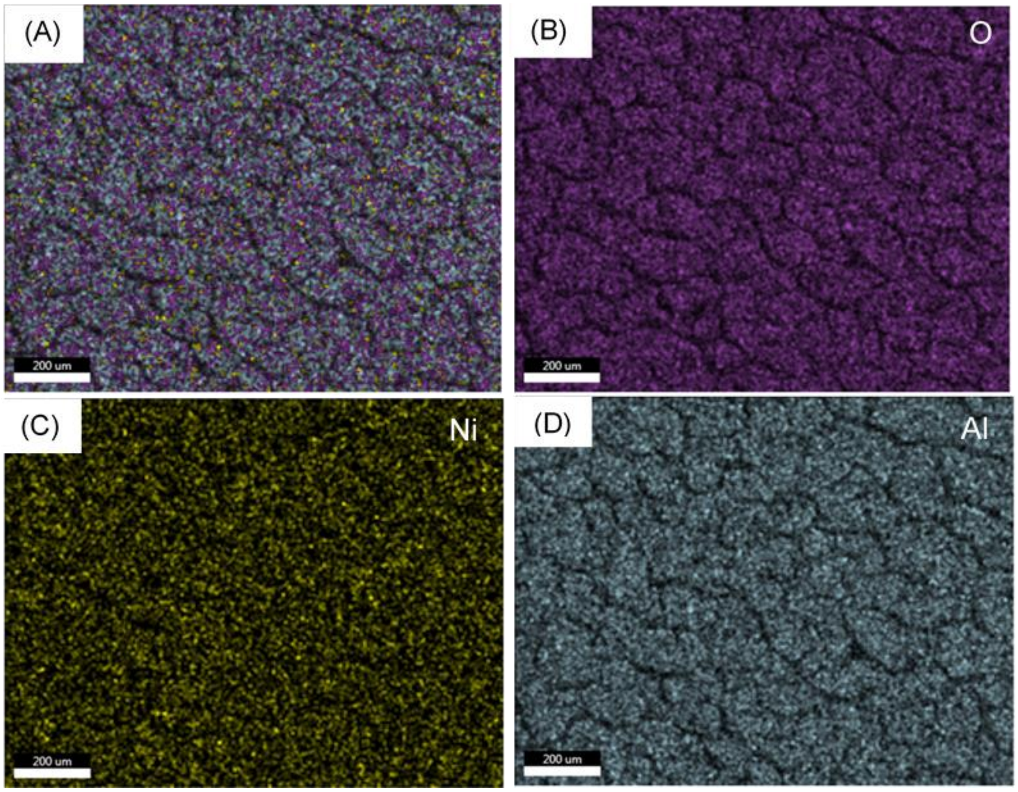

Figure 4-26 EDX elemental mapping: (A) all elements mapping combined, (B) Oxygen mapping, (C) Nickel mapping, and (D) Aluminum mapping. Coating with slurry #6.

4.4.2 Profilometry

Air-dried between coating

Figure 4-27 shows the height profile and catalyst mass distribution of the multiple-coated plate, which was air-dried between each dip-coating (plate #89 in appendix, catalyst loading of 3.07 mg mm^{-2}). Along the center line, the coating had an average height of 18.8 μm and a catalyst distribution of 1.5 mg mm^{-1}. The 3-D mapping of the height profile confirmed the homogeneity of the coating over the whole area. The larger catalyst amount at the beginning of the coating was due to surface tension effects at the tape. Mass distribution (ω_{cat}) can be calculated using the following formula.

$$\omega_{cat} = \frac{m_{\Delta x_i}}{\Delta x_i} = \frac{h(x_i)}{\int_{X_i}^{X_c} h(x)dx} \cdot m_{cat}$$

Where, $m_{\Delta x_i}$ represents the mass of the catalyst over an interval i, $\Delta \mathrm{x_i}$ is the interval width, $m_{cat}$is the mass of the catalyst on the plate, and $h(x_i)$ is the average measured height over interval i.

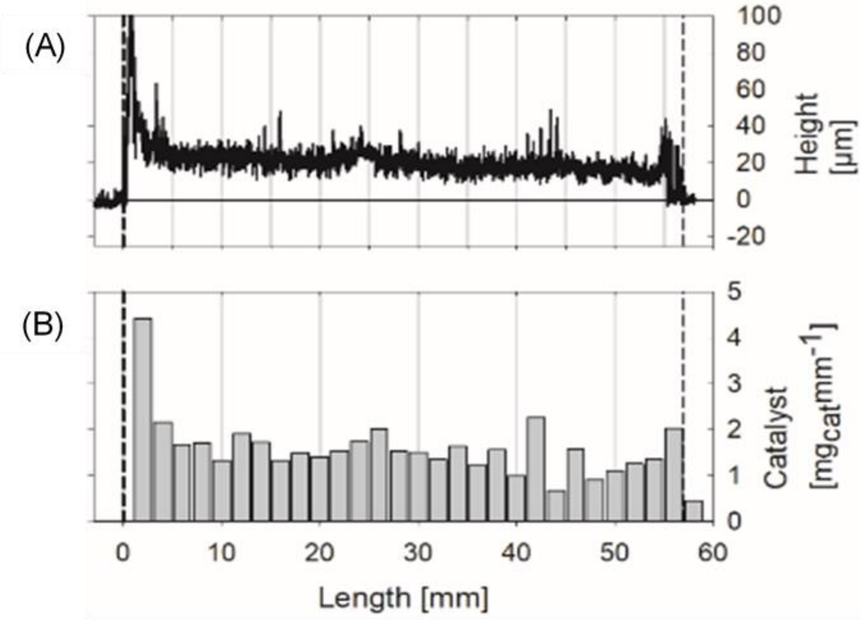

Figure 4-27 (A) Height profile of catalyst coating air-dried between dip-coating, (B) Catalyst mass distribution of catalyst coating air-dried between dip-coating.

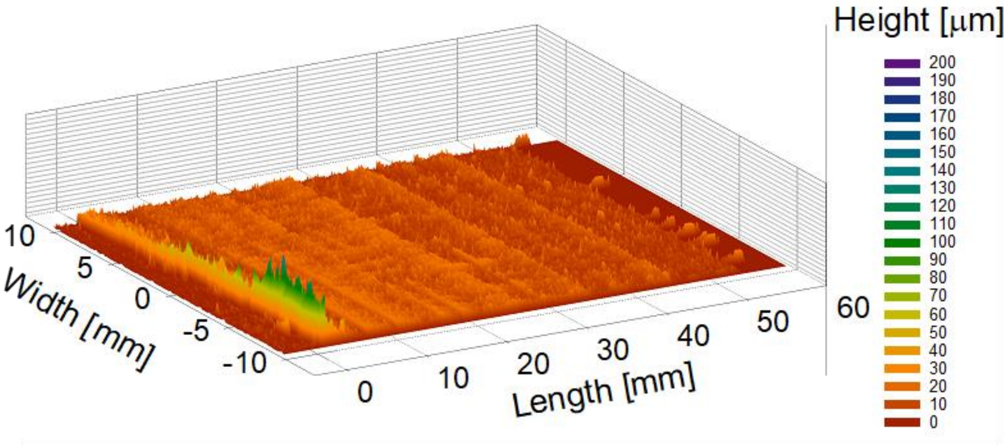

Figure 4-28 3D-mapping of height profile of catalyst coating air-dried between dip-coating.

Mild calcination between coatings

Figure 4-29 shows the height profile and catalyst mass distribution of the multiple coated plate that was calcined at 100°C for 30 min in between each dip-coating (plate #123 in appendix, catalyst loading of 3.37 mg mm^{-2}). An average height of 25 µm and catalyst mass distribution of 1.3 mg mm^{-1} was determined along the center line. This coating was more homogenous than the air-dried coating. The mass distribution of the mildly calcined coating was less than that of the air dried coating because the mass distribution profile was measured only at the center line and the air dried coating's mass distribution fluctuated due to its unevenness. Figure 4-30 shows the 3-D mapping of the mildly calcined coating which has a height profile of 25 µm, with some parts of the coating reaching more than 30 µm.

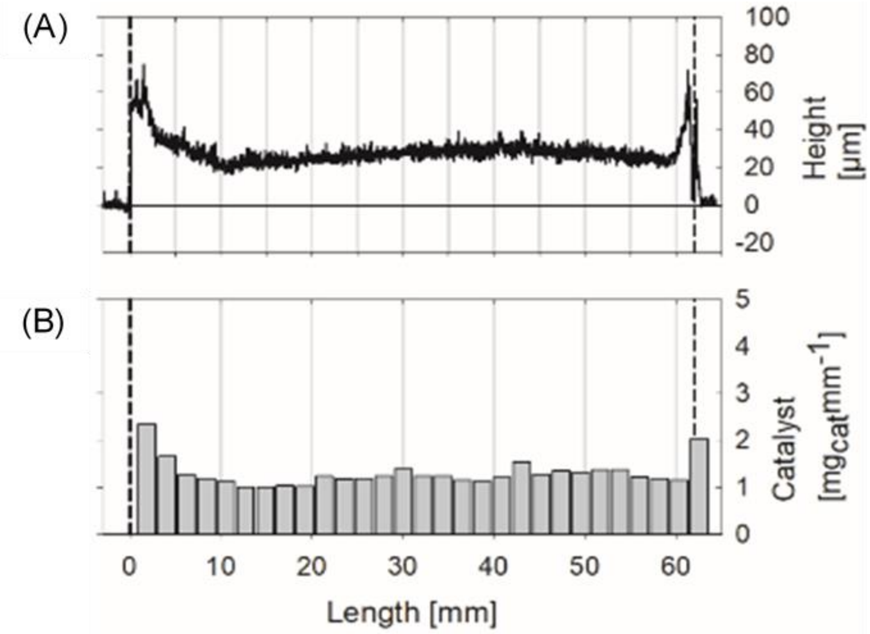

Figure 4-29 (A) Height profile and (B) catalyst mass distribution of catalyst coating calcined at 100°C between dip-coating.

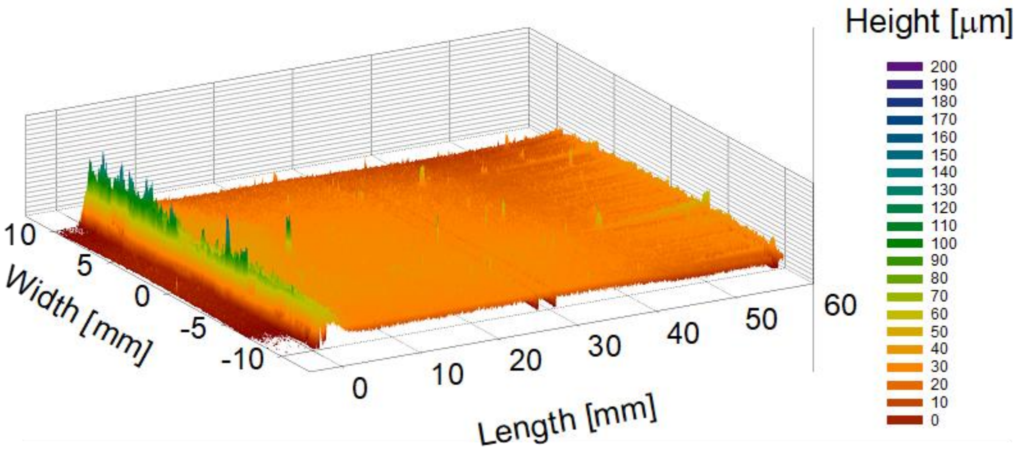

Figure 4-30 3-D mapping of height profile of catalyst coating calcined at 100°C between dip-coating.

Comparison to other coating methods

Our research group has already tested other methods of catalyst coating on Fecralloy plates, namely brush coating, spin coating, and frame coating done by Jose Hernandez Lalinde and JingSi Jiang (Figure 4-31) [40]. Coatings obtained by dip-coating were compared to those other methods.

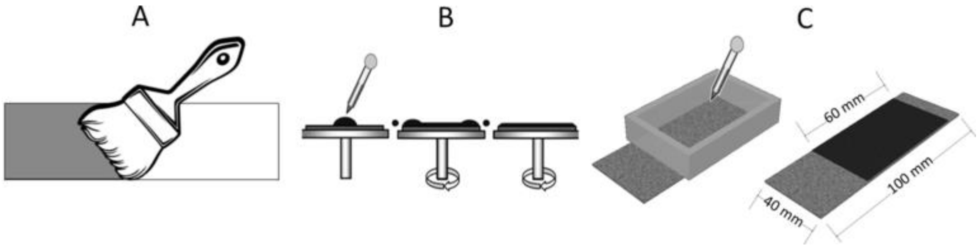

Figure 4-31 Simplified scheme of (A) brush coating, (B) spin coating and (C) frame coating [40]. Copyright (2019), with permission from Elsevier.

Figure 4-32 shows the 3-D mapping of a catalyst coating on a Fecralloy plate done using brush coating. This method consists of painting the catalyst slurry onto the surface manually using a brush. The coating was erratic and uneven with a height profile of ~10-20 µm. This is lower than the profile achieved by the multiple dip-coating method.

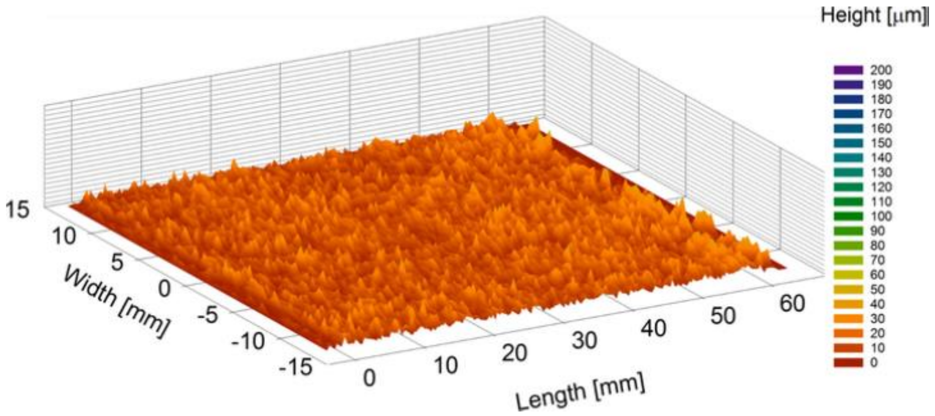

Figure 4-32 3-D mapping of height profile of catalyst coating done by brush coating on Fecralloy plate [40]. Copyright (2019), with permission from Elsevier.

Figure 4-33 depicts the 3-D mapping of the catalyst coating height profile done by spin-coating on a Fecralloy plate. The slurry was deposited onto the center of the plate which was then spun for the coating to be dispersed over the plate via centrifugal force. However, compared to coatings done using the dip-coating method, the coatings obtained by spin coating were not as evenly distributed. Most of the slurry mass remained at the center of the plate.

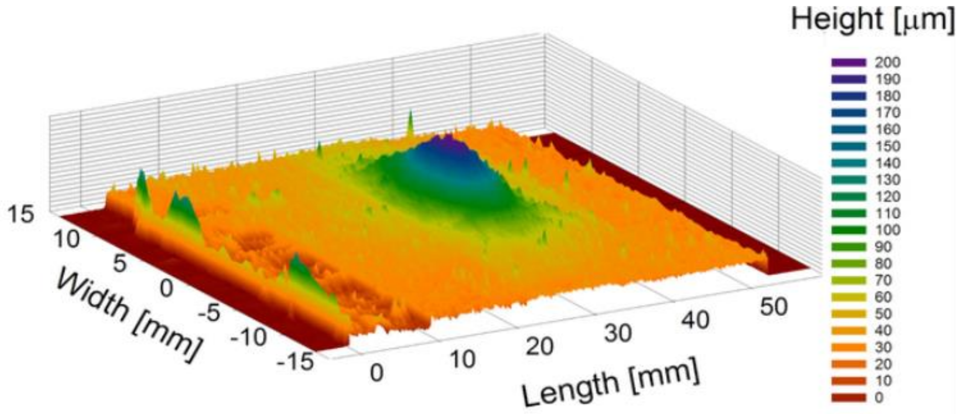

Figure 4-33 3-D mapping of height profile of catalyst coating done by spin coating on Fecralloy plate [40]. Copyright (2019), with permission from Elsevier.

Figure 4-34 shows the 3-D mapping of the frame coated catalyst slurry on an Fecralloy plate. Liquid slurry was poured onto the plate which was framed to define the area that needed to be coated. The coating done via frame coating was very even and homogenous with an excellent mass distribution. The frame coated plate had a height profile of ~30-40 μm. This is greater than the height profile of ~25 μm obtained from dip-coating. However, dip-coating allows for the plate to be coated on both sides, which will prove beneficial in developing a channel reactor. Additionally, the catalyst loading, and height profile of the samples can be increased by dip-coating the plates multiple times.

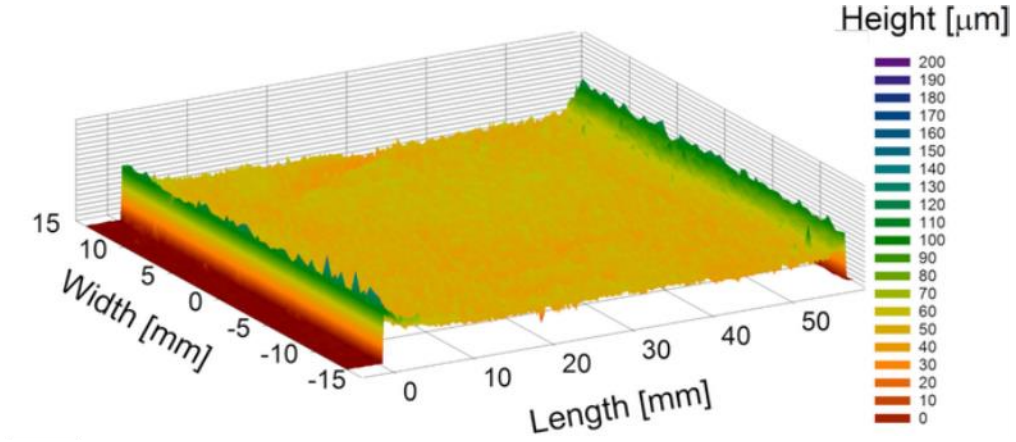

Figure 4-34 3-D mapping of height profile of catalyst coating done by frame coating on Fecralloy plate [40]. Copyright (2019), with permission from Elsevier.

4.4.3 Mechanical test

Short term test

A large 4 x 10 cm chemically treated plate that had been coated multiple times with a mild calcination at 100°C between each coating was subjected to a short term mechanical test under a 600 $ml_N\ min^{-1}$ Ar flow for 1 h. Figure 4-35 shows the coating on the plate before and after the test. After 1 h, the coating showed no signs of significant change or loss. Moreover, after comparing the weight of the plate before and after the test, it was discovered that the flowing of Ar gas caused no loss of coating.

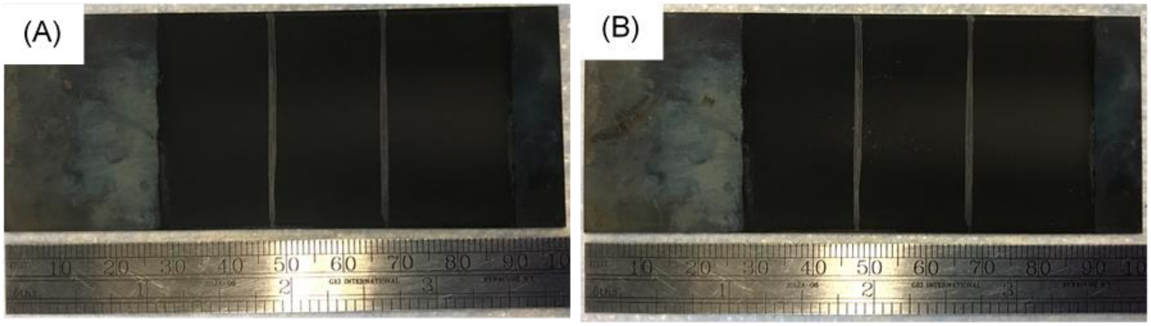

Figure 4-35 Multiple-coated plate with mild calcination between coating (A) Before Mechanical test, (B) After mechanical test under 600 ml_N min^{-1} Ar flow rate for 1 h.

Long term test

A long term mechanical test (500 h) was done to investigate the multiple coating with mild calcination method on different substrate metal plates. A 2.5 x 10 cm stainless steel plate and a Fe-Cr alloy plate were chemically treated in a 30 wt% H_2SO_4 solution for 2 h (plate #124 and #125 in appendix), while another Fecralloy plate was thermally treated at 1000°C for 24 h (plate #126 in appendix). The plates were dip-coated 12 times with a mild calcination at 100°C for 30 min between each coating. Figure 4-36 shows pictures of the plates after coating and post-calcination.

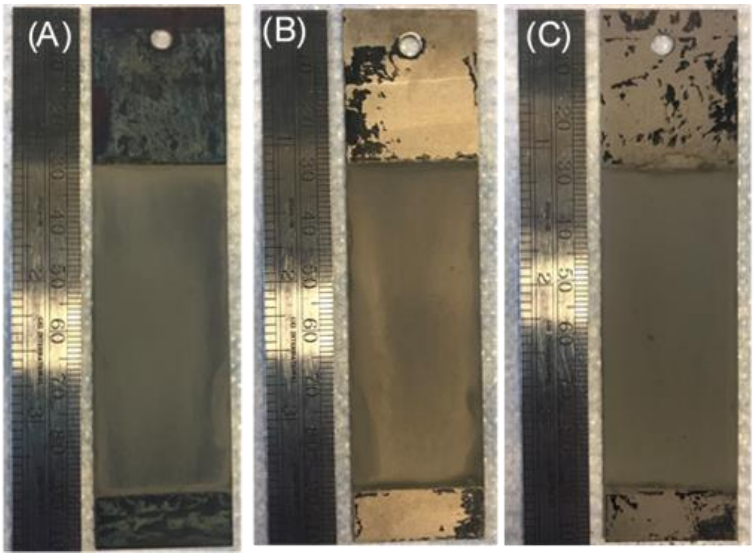

Figure 4-36 Pictures of coated plates before long term mechanical test. (A) Chemically treated stainless steel, (B) chemically treated Fecralloy, and (C) thermally treated Fecralloy.

After 500 h at 400°C under Ar flow (100 - 430 ml_N min^{-1}), no significant loss of coating occurred as shown in Figure 4-37. However, once the plates were weighed and compared, it was noticed that some coating was lost after the long period of heating under Ar flow as shown in Table 4-5. The chemically and thermally treated Fe-Cr alloy plates lost 4.4 mg and 2.0 mg of catalyst respectively. The stainless steel plate lost only 0.1 mg, the lowest amount of coating lost between the three plates. Unfortunately, due to the time consuming nature of the test, the experiment was not replicated.

Table 4-4 Weight loss of catalyst coating after long-term test.

No.	Substrate	Pre-treat method	Before [g]	After [g]	Weight loss [mg]
1	Stainless steel	30 wt% H_2SO_4 2 h	8.0823	8.0822	0.1
2	FeCrAlloy	30 wt% H_2SO_4 2 h	6.2483	6.2439	4.4
3	FeCrAlloy	Calcined at 1000°C 24 h	9.0225	9.0205	2.0

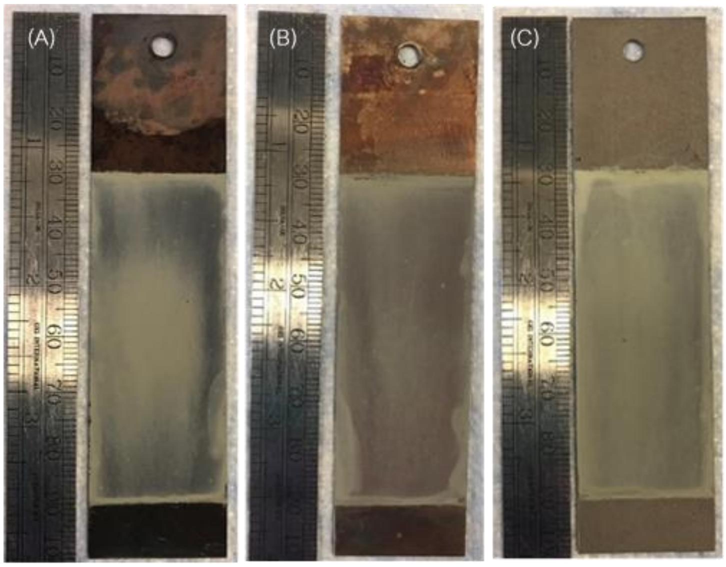

Figure 4-37 Pictures of coated plates after 500 h test. (A) Chemically treated stainless steel, (B) chemically treated Fecralloy, and (C) thermally treated Fercalloy.

4.5 Activity measurement

CO_2 methanation activity measurements were done by placing the catalyst coating plate (slurry #6) into the catalytic plate reactor (CPR). A 4x10 cm stainless steel plate, which had been dip-coated 14 times under a mild calcination at a temperature of 100°C for 30 min between coatings was used (plate #123 in appendix). Slurry #6 was selected as it had provided the highest catalyst loading amongst all the prepared slurries and had the most even and homogenous coating. The coated plate was placed inside the CPR where the catalyst coating was reduced and subsequently tested over a temperature range of 300-400°C. In each experiment, 64 $ml_N\ min^{-1}$ H_2, 16 $ml_N\ min^{-1}$ CO_2, and 20 $ml_N\ min^{-1}$ Ar were fed, while the gas composition and catalyst surface temperature profiles were acquired (Figures 4-38 to 4-40). Table 4-6 summarizes the CO_2 conversion (X_{CO_2}) and CH_4 selectivity (S_{CH_4}) measured at the outlet of the reactor.

Table 4-5 CO_2 conversion and CH_4 selectivity of methanation reaction catalyzed by catalyst coating under different temperature.

Experiment	**Temperature [°C]**	**X_{CO_2} [%]**	**S_{CH_4} [%]**
1	300	6.2	92.8
2	320	10.0	92.8
3	340	17.4	92.2
4	360	23.9	92.3
5	380	32.8	91.4
6	400	37.4	90.5

The CO_2 conversion was of 6.2% at 300°C. Once the reactor temperature was set to a maximum of 400°C, CO_2 conversion increased to 37.4%, which is around 6-7 times more. However, a trend of decreasing CH_4 selectivity was also observed with increasing temperature. At 300°C, CH_4 selectivity was 92.8%, while at 400°C, CH_4 selectivity was 90.5%. This is due to the formation of CO via the reverse water gas shift reaction (Rx 2; $CO_2 + H_2 \rightarrow CO + H_2O$) at higher temperatures.

Figures 4-38 to 4-40 illustrate nicely the spatial profiles of the surface temperature and gas composition. For the former, the temperature differences (i.e., before and while adding CO_2) were plotted to indicate possible changes due to the exothermicity of the reactions. For every reaction temperature tested, the temperature difference gradually increased (up to 2°C at 400°C, Figure 4-40) from the start to the middle of the coating. Thereafter, the temperature difference declined due to a slower reaction rate. The highest temperature increase was observed at the spatial location where the slope of the H_2 and CO_2 conversions were the highest (i.e., fastest CO_2 methanation rate).

The gas composition profiles nicely illustrate the decrease in H_2 and CO_2, and the increase in CH_4 and H_2O along the reactor axis over the coated area. Prior to reaching the coated area, the gas composition did not change as expected. The ratio between the amount of produced H_2O and CH_4 corresponded to the stoichiometric coefficient of 2 ($CO_2 + 4\ H_2 \rightarrow CH_4 + 2\ H_2O$). Moreover, there was also slight increase of CO along the coating resulting from the reversed water gas shift reaction ($CO_2 + H_2 \rightarrow CO + H_2O$). With increasing temperature (from 300 to 400°C) the slopes of the H_2 and CO_2 conversion peaks and CH_4 and H_2O formation rates increased, indicating a faster reaction rate. Moreover, as the reaction temperature increased, the amount of CO increased as well resulting in a smaller selectivity for the desired CH_4 product.

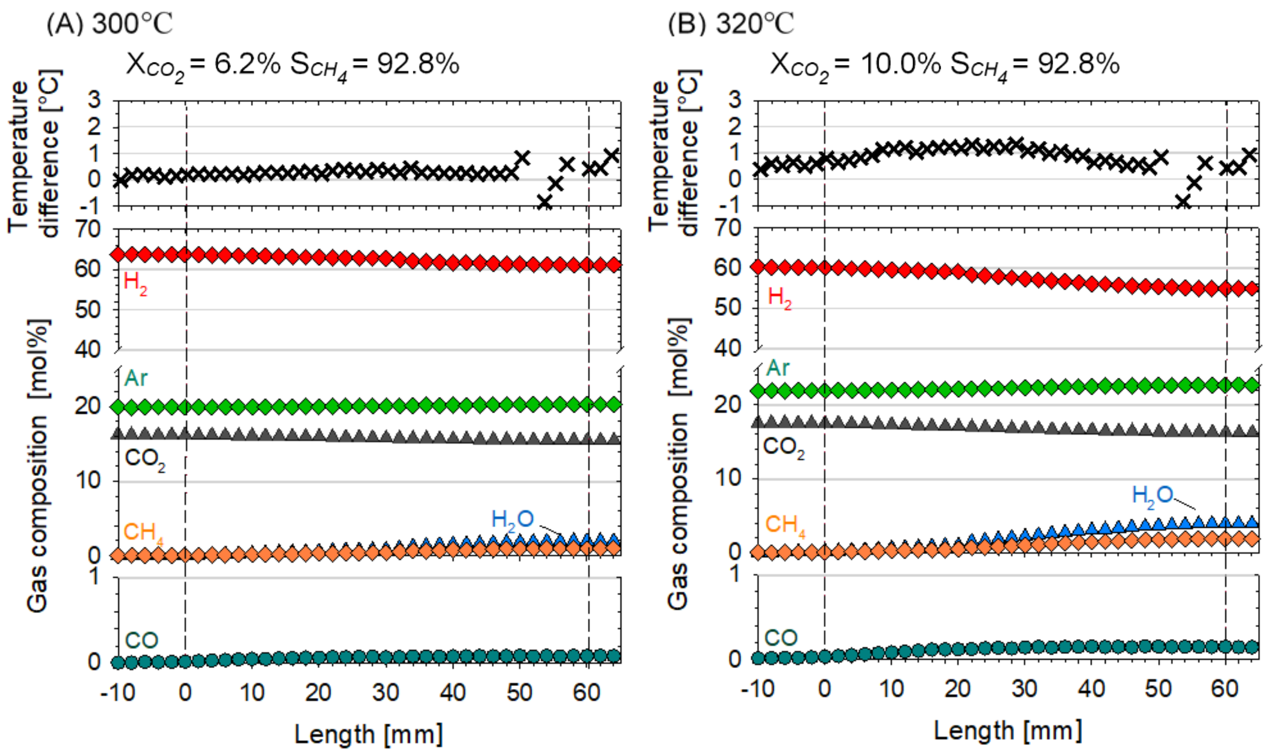

Figure 4-38 Gas composition profiles and coating temperature differences at 300 and 320°C.

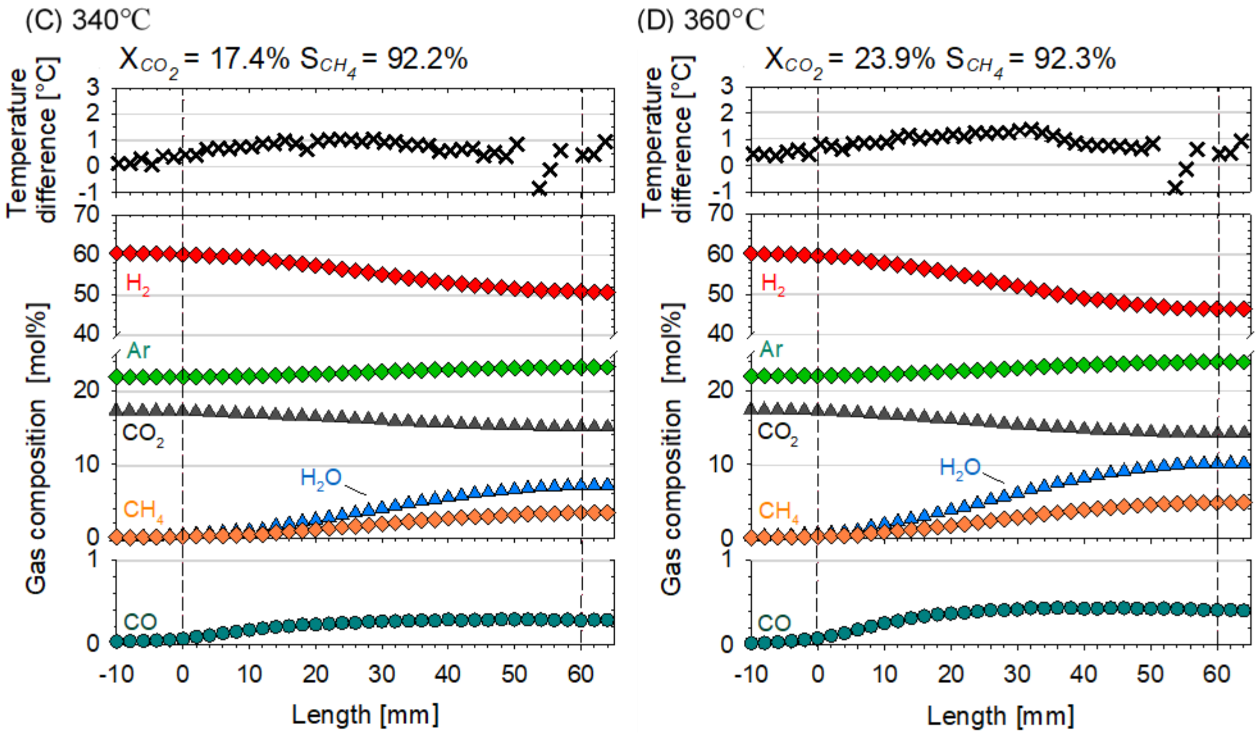

Figure 4-39 Gas composition profiles and coating temperature differences at 340 and 360°C.

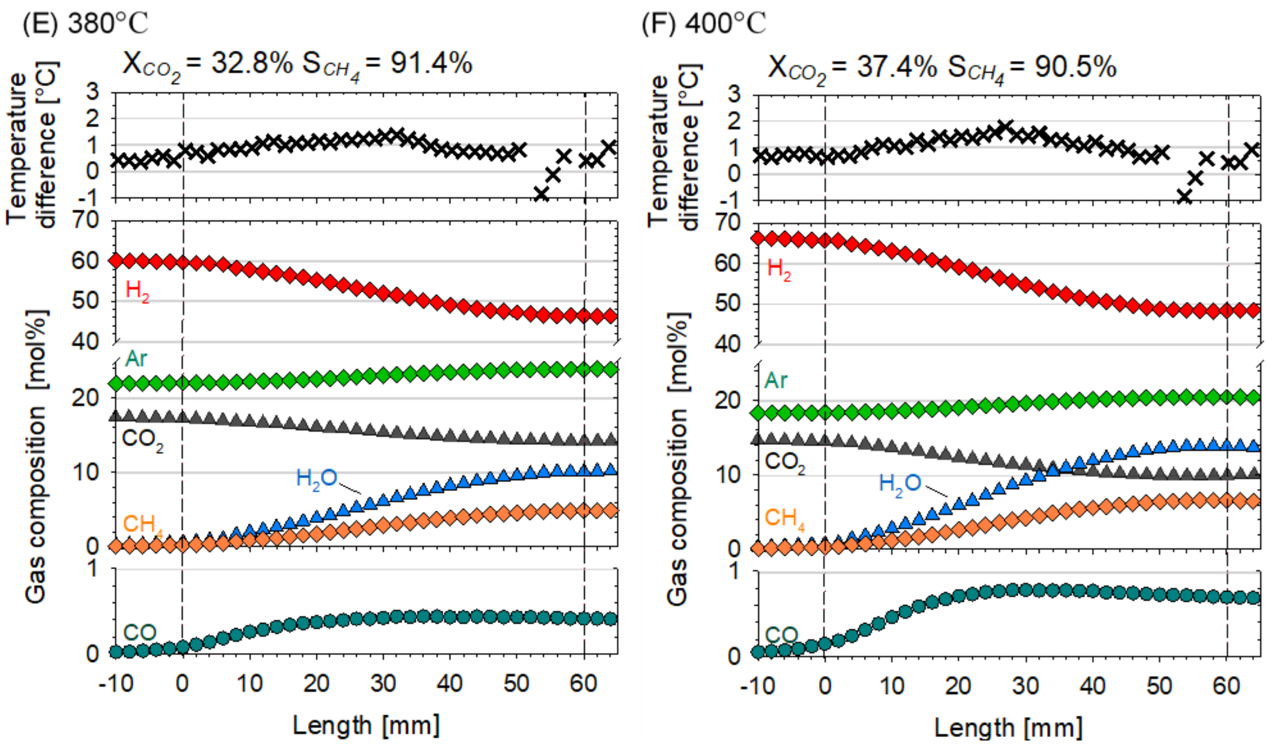

Figure 4-40 Gas composition profiles and coating temperature differences at 380 and 400°C.

Figure 4-41 depicts the homogeneous catalyst surface temperature's 2D profile gathered during CO_2 methanation at 340°C. As it can be seen, the catalyst was coated very homogeneously, and no hot-spots were observed.

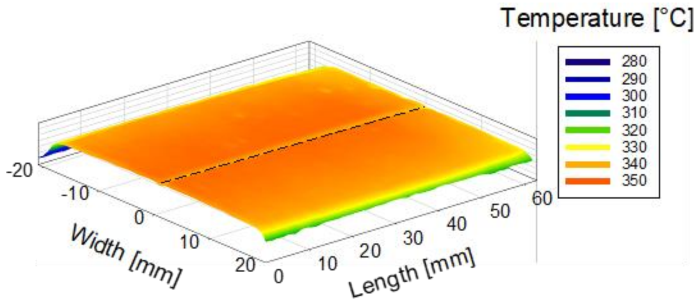

Figure 4-41 3D-temperature profile of catalyst coating under 340°C

Chapter 5

5 Conclusions and recommendations

5.1 Conclusions

This research focused on investigating process parameters that affect the coating of commercial nickel catalysts onto stainless steel substrate plates. The aim was to develop a coating procedure that would result in a homogeneous and strong coating with a known and tunable catalyst mass distribution.

As per the first objective, three different substrate pre-treatment methods were investigated. Chemical treatment in 30 wt% H_2SO_4 produced the highest surface roughness and yielded the highest catalyst loading (1.7 mg cm^{-2}) when compared to samples that underwent thermal and mechanical treatment. Binder, nitric acid and polyvinyl alcohol were needed in the slurry preparation to assure a proper suspension of the catalyst particles.

Furthermore, the smaller the particle size and the higher the solid content in the slurry, the higher the final catalyst loading became. Catalyst particles of less than 20 μm were preferred. Slurries with lower catalyst content and lower viscosity (152 cP) yielded a very small catalyst loading after a single dip-coating. Thus, multiple dip-coating steps with intermediate calcination at 100°C are needed to achieve a homogenous coating with a desired catalyst loading of 3 mg cm^{-2}.

The catalyst slurry preparation did not alter the properties of the catalyst, as the H_2-uptakes and active surface areas were the same for both the fresh catalyst and the slurry. However, due to the addition of a binder and sonication, the total surface area was larger than that of the fresh catalyst.

The multiple dip-coated stainless steel plates were mechanically very stable as proven with the 500 h test under hot flow conditions.

In summary, an optimized dip-coating process was developed that yielded a very homogenous and strong coating with a known catalyst mass distribution. Thus, the plates were ideal for use in a catalytic channel reactor for CO_2 methanation as shown with the spatially-resolved measurements conducted between 300-400°C. With increasing temperature, the CO_2 conversion increased while the CH_4 selectivity decreased due to formation of CO via the reverse water gas shift reaction.

5.2 Recommendations for future work

Further activity measurements of the catalyst coated plates should be done to collect more kinetic data. That includes experiments with different pressures (1-10 bar), H_2/CO_2 ratio and co-feeds such as CH_4, CO and H_2O. The latter experiments are important to investigate the possible inhibition effects of the reaction products on CO_2 methanation. The data would be used for kinetic parameter estimation and model discrimination which are essential for the designing of the prototype channel reactor. The next step of this research is to implement the optimized multiple dip-coating method towards larger stainless steel plates to construct a microchannel reactor. In addition, the dip-coating method needs to be tested with corrugated and channeled stainless steel plates to investigate the effect of plate shape on the quality of the coating and quantity of catalyst loading.

References

[1] L. Bird, M. Milligan, and D. Lew, "Integrating Variable Renewable Energy: Challenges and Solutions," 2013.

[2] "Technology Roadmap," *Encycl. Prod. Manuf. Manag.*, pp. 781–782, 2006.

[3] G. Cooley, "Power-to-gas: storing renewable energy in the gas grid," 2014.

[4] M. Sterner, Institut für Solare Energieversorgungstechnik., and Institut für Elektrische Energietechnik Rationelle Energiewandlung., *Bioenergy and renewable power methane in integrated 100% renewable energy systems : limiting global warming by transforming energy systems*. Kassel University Press, 2009.

[5] M. Lehner, R. Tichler, H. Steinmüller, and M. Koppe, *Power-to-Gas: Technology and Business Models*. Cham: Springer International Publishing, 2014.

[6] K. Stangeland, D. Kalai, H. Li, and Z. Yu, "CO2 Methanation: The Effect of Catalysts and Reaction Conditions," in *Energy Procedia*, 2017, vol. 105, pp. 2022–2027.

[7] M. Zanfir and A. Gavriilidis, "Catalytic combustion assisted methane steam reforming in a catalytic plate reactor," *Chem. Eng. Sci.*, vol. 58, no. 17, pp. 3947–3960, Sep. 2003.

[8] P. Lakhete and V. M. Janardhanan, "Modeling process intensified catalytic plate reactor for synthesis gas production," *Chem. Eng. Sci.*, vol. 110, pp. 13–19, May 2014.

[9] G. A. Mills and F. W. Steffgen, "Catalytic methanation," *Catal. Rev.*, vol. 8, no. 1, pp. 159–210, 1974.

[10] M. Ascencio, "Evaluation and design of a novel CO2 methanation reactor integrated into a Biogas upgrading facility," 2016.

[11] J. Kopyscinski, T. J. Schildhauer, and S. M. A. Biollaz, "Production of synthetic natural gas (SNG) from coal and dry biomass – A technology review from 1950 to 2009," *Fuel*, vol. 89, no. 8, pp. 1763–1783, Aug. 2010.

[12] T. A. Nijhuis, A. E. W. Beers, T. Vergunst, I. Hoek, F. Kapteijn, and J. A. Moulijn, "Preparation of monolithic catalysts," *Catal. Rev.*, vol. 43, no. 4, pp. 345–380, Nov. 2001.

[13] J. Kopyscinski, *Production of synthetic natural gas in a fluidized bed reactor Understanding the hydrodynamic, mass transfer, and kinetic effects*. Suedwestdeutscher Verlag fuer Hochschulschriften, 2010.

[14] V. Meille, "Review on methods to deposit catalysts on structured surfaces," *Appl. Catal. A Gen.*, vol. 315, pp. 1–17, Nov. 2006.

[15] J. Gao, Q. Liu, F. Gu, B. Liu, Z. Zhong, and F. Su, "Recent advances in methanation catalysts for the production of synthetic natural gas," *RSC Adv.*, vol. 5, no. 29, pp. 22759–22776, Feb. 2015.

[16] M. A. Vannice, "The catalytic synthesis of hydrocarbons from H2 CO mixtures over the group VIII metals. I. The specific activities and product distributions of supported metals," *J. Catal.*, vol. 37, no. 3, pp. 449–461, Jun. 1975.

[17] P. Ciambelli, V. Palma, and E. Palo, "Comparison of ceramic honeycomb monolith and foam as Ni catalyst carrier for methane autothermal reforming," *Catal. Today*, vol. 155, no. 1–2, pp. 92–100, Oct. 2010.

[18] D. Hu *et al.*, “Enhanced Investigation of CO Methanation over Ni/Al 2 O 3 Catalysts for Synthetic Natural Gas Production,” *Ind. Eng. Chem. Res.*, vol. 51, no. 13, pp. 4875–4886, Apr. 2012.

[19] G. Garbarino, I. Valsamakis, P. Riani, and G. Busca, “On the consistency of results arising from different techniques concerning the nature of supported metal oxide (nano)particles. the case of NiO/Al 2O3,” *Catal. Commun.*, vol. 51, pp. 37–41, Jun. 2014.

[20] I. Czekaj, F. Loviat, F. Raimondi, J. Wambach, S. Biollaz, and A. Wokaun, “Characterization of surface processes at the Ni-based catalyst during the methanation of biomass-derived synthesis gas: X-ray photoelectron spectroscopy (XPS),” *Appl. Catal. A Gen.*, vol. 329, pp. 68–78, Oct. 2007.

[21] “Fecralloy® - Iron/Chromium - online catalogue source - supplier of research materials in small quantities - Goodfellow.” [Online]. Available: http://www.goodfellow.com/E/Fecralloy-Iron-Chromium.html. [Accessed: 01-Nov-2017].

[22] J. Camra *et al.*, “Role of Al segregation and high affinity to oxygen in formation of adhesive alumina layers on FeCr alloy support,” *Catal. Today*, vol. 105, no. 3–4, pp. 629–633, Aug. 2005.

[23] C. Cristiani, M. Valentini, M. Merazzi, S. Neglia, and P. Forzatti, “Effect of ageing time on chemical and rheological evolution in ??-Al2O3 slurries for dip-coating,” in *Catalysis Today*, 2005, vol. 105, no. 3–4, pp. 492–498.

[24] N. de Miguel, J. Manzanedo, J. Thormann, P. Pfeifer, and P. L. Arias, “Ni Catalyst Coating on Fecralloy ® Microchanneled Foils and Testing for Methane Steam Reforming,” *Chem. Eng. Technol.*, vol. 33, no. 1, pp. 155–166, Jan. 2010.

[25] “Ceramics - Industrial Ceramics and Glass - Goodfellow-Ceramics,” 2014. [Online]. Available: http://www.goodfellow-ceramics.com/products/ceramics/. [Accessed: 01-Nov-2017].

[26] P. Jiang, G. Lu, Y. Guo, Y. Guo, S. Zhang, and X. Wang, “Preparation and properties of a γ-Al2O3 washcoat deposited on a ceramic honeycomb,” *Surf. Coatings Technol.*, vol. 190, no. 2–3, pp. 314–320, Jan. 2005.

[27] “The basic information about stainless steel: how it’s made, why it’s useful and what it’s used for.” [Online]. Available: http://www.bssa.org.uk/about_stainless_steel.php. [Accessed: 02-Nov-2017].

[28] M. Khodadadi-Moghaddam, F. Salimi, L. Jamshidi, N. Jafari, and H. Sahebalzamani, “Solvent effects in esterification of phthalic anhydride on sulfated titania-based solid acid,” *J. Sulfur Chem.*, vol. 32, no. 6, pp. 533–541, Dec. 2011.

[29] R. Sánchez-Tovar, R. Leiva-García, and J. García-Antón, “Characterization of thermal oxide films formed on a duplex stainless steel by means of confocal-Raman microscopy and electrochemical techniques,” *Thin Solid Films*, vol. 576, pp. 1–10, Feb. 2015.

[30] Y. Gong *et al.*, “On the breakaway oxidation of Fe9Cr1Mo steel in high pressure CO2,” *Acta Mater.*, vol. 130, pp. 361–374, May 2017.

[31] M. Valentini, G. Groppi, C. Cristiani, M. Levi, E. Tronconi, and P. Forzatti, “The deposition of γ-Al2O3 layers on ceramic and metallic supports for the preparation of structured catalysts,” *Catal. Today*, vol. 69, no. 1–4, pp. 307–314, Sep. 2001.

[32] T. Giornelli, A. Löfberg, and E. Bordes-Richard, “Preparation and characterization of VOx/TiO2 catalytic coatings on stainless steel plates for structured catalytic reactors,” *Appl. Catal., A*, vol. 305, no. 2, pp. 197–203, May 2006.

[33] K. I. Sarwani, R. H. Madon, S. A. Ibrahim, and M. Fawzi, “Effect of Calcination Temperature on

Morphological and Topography of Nickel-Alumina Thin Film," *MATEC Web Conf.*, vol. 78, p. 01049, Oct. 2016.

[34] N. Barati, M. A. F. Sani, H. Ghasemi, Z. Sadeghian, and S. M. M. Mirhoseini, "Preparation of uniform TiO2 nanostructure film on 316L stainless steel by sol-gel dip coating," *Appl. Surf. Sci.*, vol. 255, no. 20, pp. 8328–8333, Jul. 2009.

[35] Z. Ma, F. Zaera, Z. Ma, and F. Zaera, "Heterogeneous Catalysis by Metals," in *Encyclopedia of Inorganic Chemistry*, Chichester, UK: John Wiley & Sons, Ltd, 2006.

[36] † J. R. González-Velasco, *, † M. A. Gutiérrez-Ortiz, † J. L. Marc, † J. A. Botas, † and M. P. González-Marcos, and G. Blanchard‡, "Pt/Ce0.68Zr0.32O2 Washcoated Monoliths for Automotive Emission Control," 2002.

[37] C. Agrafiotis, A. Tsetsekou, and A. Ekonomakou, "The effect of particle size on the adhesion properties of oxide washcoats on cordierite honeycombs," vol. 8, no. 9, pp. 1421–1424.

[38] N. R. Peela, A. Mubayi, and D. Kunzru, "Washcoating of γ-alumina on stainless steel microchannels," *Catal. Today*, vol. 147, pp. S17–S23, Sep. 2009.

[39] L. Zhang, Y. Ren, Q. Luo, X. Ying, H. Xu, and J. Xuan, "A Novel Method to from Well-adhered γ-Al2O3 Coating in 316L Stainless Steel Microchannels," *Energy Procedia*, vol. 75, pp. 2044–2048, Aug. 2015.

[40] J. A. H. Lalinde, J. Jiang, G. Jai, and J. Kopyscinski, "Preparation and characterization of Ni/Al2O3 catalyst coatings on FeCrAl-loy plates used in a catalytic channel reactor with in-situ spatial profiling to study CO2 methanation," *Chem. Eng. J.*, vol. 357, pp. 435–446, Feb. 2019.

[41] A. Khosravi, "The development of a metal plate test reactor for studying reaction kinetics on catalytically coated heat transfer components," 2012.

[42] S. Walter, S. Malmberg, B. Schmidt, and M. A. Liauw, "Mass transfer limitations in microchannel reactors," *Catal. Today*, vol. 110, no. 1–2, pp. 15–25, Dec. 2005.

[43] S. Kishida, D.-Y. Ju, and H. He, "Influence of coating method on catalyst activity of AgCl/Al2O3/SUS304 composite plate.," *J. Environ. Sci. (China)*, vol. 23 Suppl, pp. S90-4, Jun. 2011.

[44] "Principles of X-ray Diffraction."

[45] J. A. H. Lalinde *et al.*, "Improved Kinetic Data Acquisition Using An Optically Accessible Catalytic Plate Reactor with Spatially-Resolved Measurement Techniques. Case of Study: CO2 Methanation," *Catalysts*, vol. 8, no. 2, p. 86, Feb. 2018.

[46] R. Haul, "S. J. Gregg, K. S. W. Sing: Adsorption, Surface Area and Porosity," *Berichte der Bunsengesellschaft für physikalische Chemie*, vol. 86, no. 10. pp. 957–957, 1982.

List of Figures

List of Tables

Appendices

A1 Formula for catalyst loadings

$$m_{coating}\ [g] = m_{coated\ plate}[g] - m_{uncoated\ plate}[g]$$

$$m_{coating}\ [g\ cm^{-2}] = \frac{m_{coating}\ [g]}{m_{coated\ area}\ [cm^{2}]}$$

$$m_{actual\ catalyst}\ [g\ cm^{-2}] = m_{coating}\ [g\ cm^{-2}] \times catalyst\ to\ binder\ ratio\ in\ slurry$$

A2 List of Plates

Plate	Plate size	Slurry	Pre-treatment	Particle size	Catalyst loading	Catalyst loading	Note
no.	[cm]	no.		[µm]	[mg]	[mg/cm-2]	
1	2x4	-	T-600	-	-	-	not coated
2	2x4	-	T-700	-	-	-	not coated
3	2x4	-	T-800	-	-	-	not coated
4	2x4	-	T-900	-	-	-	not coated
5	2x4	-	M-axial	-	-	-	not coated
6	2x4	-	M-per	-	-	-	not coated
7	2x4	#1	T-600	20 - 45	3.8	0.76	homogenous coating
8	2x4	#1	T-700	20 - 45	4.4	0.88	homogenous coating
9	2x4	#1	T-800	20 - 45	4.9	0.97	homogenous coating
10	2x4	#1	T-900	20 - 45	5.8	1.15	homogenous coating
11	2x4	#1	M-axial	20 - 45	3.1	0.61	homogenous coating
12	2x4	#1	M-per	20 - 45	3.5	0.70	homogenous coating
13	2x4	#2	T-600	< 20	0.9	0.18	low loading, slurry not ready
14	2x4	#2	T-700	< 20	0.1	0.02	low loading, slurry not ready
15	2x4	#2	T-800	< 20	0.9	0.18	low loading, slurry not ready
16	2x4	#2	T-900	< 20	1.3	0.26	low loading, slurry not ready
17	2x4	#2	M-axial	< 20	0.9	0.18	low loading, slurry not ready
18	2x4	#2	M-per	< 20	0.4	0.09	low loading, slurry not ready
19	2x4	#2	C-10	< 20	0.7	0.14	low loading, slurry not ready
20	2x4	#2	C-20	< 20	0.8	0.16	low loading, slurry not ready
21	2x4	#2	C-30	< 20	0.2	0.04	low loading, slurry not ready
22	2x4	#2	T-600	< 20	6.4	1.28	homogenous coating
23	2x4	#2	T-700	< 20	4.7	0.93	homogenous coating
24	2x4	#2	T-800	< 20	6.6	1.32	homogenous coating
25	2x4	#2	T-900	< 20	4.7	0.95	homogenous coating
26	2x4	#2	M-axial	< 20	6.2	1.25	homogenous coating
27	2x4	#2	M-per	< 20	7.0	1.41	homogenous coating
28	2x4	#2	C-10	< 20	6.8	1.35	homogenous coating
29	2x4	#2	C-20	< 20	8.8	1.76	homogenous coating
30	2x4	#2	C-30	< 20	7.3	1.46	homogenous coating
31	2x4	#2	T-600	< 20	0.4	0.09	homogenous coating later cracked
32	2x4	#2	T-700	< 20	5.9	1.18	homogenous coating later cracked
33	2x4	#2	T-800	< 20	5.8	1.16	homogenous coating
34	2x4	#2	T-900	< 20	0.6	0.12	homogenous coating
35	2x4	#2	M-axial	< 20	8.4	1.67	homogenous coating later cracked
36	2x4	#2	M-per	< 20	4.7	0.93	homogenous coating later cracked
37	2x4	#2	C-10	< 20	8.2	1.64	uneven

Plate	**Plate size**	**Slurry**	**Pre-treatment**	**Particle size**	**Catalyst loading**	**Catalyst loading**	**Note**
no.	**[cm]**	**no.**		**[µm]**	**[mg]**	**[mg cm^{-2}]**	
38	2x4	#2	C-20	< 20	7.2	1.44	homogenous coating
39	2x4	#2	C-30	< 20	8.4	1.69	homogenous coating
40	2x4	#2	T-600	< 20	3.6	0.72	homogenous coating later cracked
41	2x4	#2	T-700	< 20	5.2	1.04	uneven
42	2x4	#2	T-800	< 20	4.5	0.90	homogenous coating
43	2x4	#2	T-900	< 20	6.3	1.27	homogenous coating
44	2x4	#2	M-axial	< 20	2.6	0.51	homogenous coating later cracked
45	2x4	#2	M-per	< 20	3.5	0.70	homogenous coating later cracked
46	2x4	#2	C-10	< 20	7.5	1.50	uneven
47	2x4	#2	C-20	< 20	6.7	1.34	uneven
48	2x4	#2	C-30	< 20	10.1	2.02	homogenous coating
49	2x4	#7, #8	T-600	45 - 90	0.8	0.16	low loading and uneven
50	2x4	#7, #8	T-700	45 - 90	1.7	0.34	low loading and uneven
51	2x4	#7, #8	T-800	45 - 90	0.5	0.10	low loading and uneven
52	2x4	#7, #8	T-900	45 - 90	0.9	0.18	low loading and uneven
53	2x4	#7, #8	M-axial	45 - 90	0.9	0.18	low loading and uneven
54	2x4	#7, #8	M-per	45 - 90	1.1	0.22	low loading and uneven
55	2x4	#7, #8	C-10	45 - 90	0.9	0.18	low loading and uneven
56	2x4	#7, #8	C-20	45 - 90	0.3	0.06	low loading and uneven
57	2x4	#7, #8	C-30	45 - 90	0.2	0.04	low loading and uneven
58	2x4	#5	T-600	45 - 90	2.2	0.44	Low loading
59	2x4	#5	T-700	45 - 90	2.7	0.54	low loading and uneven
60	2x4	#5	T-800	45 - 90	0.6	0.12	low loading and uneven
61	2x4	#5	T-900	45 - 90	2.0	0.40	low loading and uneven
62	2x4	#5	M-axial	45 - 90	1.6	0.31	uneven with holes
63	2x4	#5	M-per	45 - 90	1.7	0.33	uneven with holes
64	2x4	#5	C-10	45 - 90	4.1	0.82	uneven with holes
65	2x4	#5	C-20	45 - 90	4.0	0.81	uneven with holes
66	2x4	#5	C-30	45 - 90	4.9	0.98	uneven with holes
67	2x4	#4	T-600	20 - 45	9.9	1.98	uneven
68	2x4	#4	T-700	20 - 45	12.6	2.52	homogenous coating
69	2x4	#4	T-800	20 - 45	12.8	2.55	homogenous coating
70	2x4	#4	T-900	20 - 45	8.2	1.64	uneven
71	2x4	#4	M-axial	20 - 45	7.5	1.50	uneven
72	2x4	#4	M-per	20 - 45	9.8	1.96	homogenous coating
73	2x4	#4	C-10	20 - 45	23.0	4.60	uneven slightly cracked
74	2x4	#4	C-20	20 - 45	11.1	2.22	uneven
75	2x4	#4	C-30	20 - 45	7.9	1.57	uneven
76	2x4	#3	T-600	< 20	20.3	4.06	uneven cracked

Plate	Plate size	Slurry	Pre-treatment	Particle size	Catalyst loading	Catalyst loading	Note
no.	[cm]	no.		[µm]	[mg]	[mg cm^{-2}]	
77	2x4	#3	T-700	< 20	10.3	2.11	uneven cracked
78	2x4	#3	T-800	< 20	10.3	2.72	uneven cracked
79	2x4	#3	T-900	< 20	12.5	2.50	uneven cracked
80	2x4	#3	M-axial	< 20	10.7	3.05	uneven cracked
81	2x4	#3	M-per	< 20	8.0	3.62	uneven cracked
82	2x4	#3	C-10	< 20	16.8	3.50	uneven cracked
83	2x4	#3	C-20	< 20	19.4	4.05	uneven cracked
84	2x4	#3	C-30	< 20	18.0	3.60	uneven cracked
85	4x10	#3	C-30	< 20	35.4	1.47	uneven heavily cracked
86	4x10	#6	C-30	< 20	5.4	0.23	only one thin coating
87	4x10	#6	C-30	< 20	3.9	0.16	only one thin coating
88	4x10	#6	C-30	< 20	3.1	0.13	only one thin coating
89	4x10	#6	C-30	< 20	73.6	3.07	homogenous, cracked at beginning
90	4x10	#6	C-30	< 20	77.5	3.23	homogenous, cracked at beginning
91	4x10	#6	C-30	< 20	83.1	3.46	homogenous, cracked at beginning
92	2x4	#6	T-600	< 20	0.0	0.00	homogenous low loading
93	2x4	#6	T-700	< 20	0.9	0.18	homogenous low loading
94	2x4	#6	T-800	< 20	0.5	0.11	homogenous low loading
95	2x4	#6	T-900	< 20	0.4	0.07	homogenous low loading
96	2x4	#6	M-axial	< 20	0.4	0.07	homogenous low loading
97	2x4	#6	M-per	< 20	0.3	0.05	homogenous low loading
98	2x4	#6	C-10	< 20	1.4	0.27	homogenous low loading
99	2x4	#6	C-20	< 20	2.4	0.49	homogenous low loading
100	2x4	#6	C-30	< 20	2.3	0.47	homogenous low loading
101	2x4	#6	T-600	< 20	0.4	0.07	homogenous low loading
102	2x4	#6	T-700	< 20	0.0	0.00	homogenous low loading
103	2x4	#6	T-800	< 20	0.9	0.18	homogenous low loading
104	2x4	#6	T-900	< 20	0.8	0.16	homogenous low loading
105	2x4	#6	M-axial	< 20	0.5	0.11	homogenous low loading
106	2x4	#6	M-per	< 20	0.6	0.13	homogenous low loading
107	2x4	#6	C-10	< 20	1.6	0.32	homogenous low loading
108	2x4	#6	C-20	< 20	2.4	0.49	homogenous low loading
109	2x4	#6	C-30	< 20	2.2	0.43	homogenous low loading
110	2x4	#6	T-600	< 20	0.9	0.18	homogenous low loading
111	2x4	#6	T-700	< 20	0.3	0.05	homogenous low loading
112	2x4	#6	T-800	< 20	0.4	0.07	homogenous low loading
113	2x4	#6	T-900	< 20	0.4	0.09	homogenous low loading
114	2x4	#6	M-axial	< 20	0.5	0.11	homogenous low loading
115	2x4	#6	M-per	< 20	0.2	0.04	homogenous low loading
116	2x4	#6	C-10	< 20	1.5	0.31	homogenous low loading

Plate	Plate size	Slurry	Pre-treatment	Particle size	Catalyst loading	Catalyst loading	Note
no.	[cm]	no.		[µm]	[mg]	[mg cm^{-2}]	
117	2x4	#6	C-20	< 20	1.8	0.36	homogenous low loading
118	2x4	#6	C-30	< 20	2.9	0.58	homogenous low loading
119	2x4	#6	C-30	< 20	1.2	0.23	homogenous low loading
120	2x4	#6	C-30	< 20	1.1	0.22	homogenous low loading
121	2x4	#6	C-30	< 20	2.5	0.50	homogenous low loading
122	4x10	#6	C-30	< 20	82.2	3.42	homogenous, cracked at beginning
123	4x10	#6	C-30	< 20	80.8	3.37	homogenous and even coating, used in activity measurement
124	2x4	#6	C-30	< 20	27.2	1.81	homogenous and even coating
125	2x4	#6	C-30	< 20	19.7	1.31	homogenous and even coating
126	2x4	#6	T-1000	< 20	26.2	1.75	homogenous and even coating

T = thermal treatment (600-1000°C), M = mechanical treatment (axial/perpendicular), C = chemical treatment (10-30 wt% H_2SO_4).

A3 Catalyst pictures

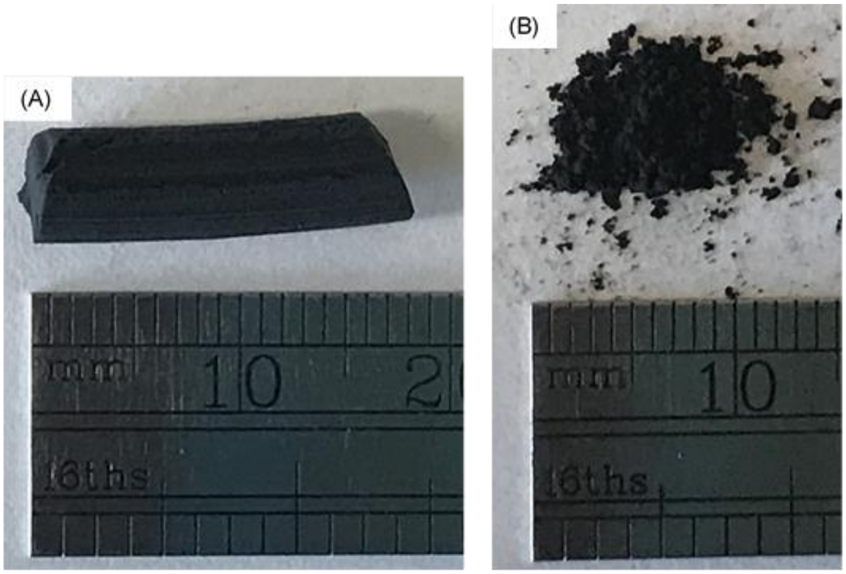

Figure A-1 Commercial catalyst 1 (A) pellet, (B) crushed and sieved.